



NTNU – Trondheim
Norwegian University of
Science and Technology

Sprekkevekst av rørsveiser under S-installasjon

Martin Aunemo Suul

Subsea Technology

Submission date: June 2013

Supervisor: Svein Sævik, IMT

Norwegian University of Science and Technology
Department of Marine Technology

MASTER THESIS SPRING 2013

for

Stud. tech. Martin Aunemo Suul

Weld Crack Growth during S-lay of Pipelines

Sprekkvekst av rørsveiser under S-installasjon

Sub-sea pipelines represent the most cost effective way of transporting oil & gas from a sub-sea field to the market. A large network of subsea pipelines has therefore been installed both at the Norwegian continental shelf and elsewhere. For large diameter pipelines (>16") S-lay is the dominant installation method. The horizontal firing line enables several welding stations and efficient pipe string production. For S-lay, a stinger is used to support the pipe until it is lowered into the sea. For this method, pipeline installation is limited by the weather window and primarily due to the motions induced at the stinger tip by 1st order wave forces on the vessel. At a certain sea state the associated cyclic bending moment may cause fatigue fracture in the weld positioned at the stinger tip. This is specially the case if the installation process is stopped for some reason thus exposing the same pipe section to many cycles. The pipe may even need to be abandoned to the seabed and later recovered when the sea state allows continued installation. The present project work focus on the fatigue crack growth of the weld at the stinger tip section.

The project work is to be carried out as follows:

1. Literature study, including pipeline technology in general i.e. pipeline manufacture & installation, associated failure modes and pipeline design procedures, rules and regulations to cope with these. A review of available models to determine the fatigue crack growth is to be included.
2. Review the theoretical background and familiarize with the Marintek computer code SIMLA and the crack growth computer program LINKPIPE.
3. Define lay scenarios with all required input for the dynamic installation and crack growth analyses pipe diameter, thickness, mechanical properties, crack growth data, strain stress curve, Vessel RAO, vessel and stinger geometry, tensioner settings.
4. Perform numerical studies with SIMLA to generate the bending moment spectrum (Classes of moment range and number of cycles)
5. Perform numerical studies with LINKPIPE to find the crack growth rate for each class.
6. Calculate the fatigue in terms of damage frequency and accumulated damage considering the joint manufacturing times.
7. Conclusions and recommendations for further work.

All input data to be provided by Reinertsen (RE) in cooperation with NTNU

The work scope may prove to be larger than initially anticipated. Subject to approval from the supervisors, topics may be deleted from the list above or reduced in extent.

In the thesis the candidate shall present his personal contribution to the resolution of problems within the scope of the thesis work

Theories and conclusions should be based on mathematical derivations and/or logic reasoning identifying the various steps in the deduction.

The candidate should utilize the existing possibilities for obtaining relevant literature.

Thesis format

The thesis should be organized in a rational manner to give a clear exposition of results, assessments, and conclusions. The text should be brief and to the point, with a clear language. Telegraphic language should be avoided.

The thesis shall contain the following elements: A text defining the scope, preface, list of contents, summary, main body of thesis, conclusions with recommendations for further work, list of symbols and acronyms, references and (optional) appendices. All figures, tables and equations shall be numerated.

The supervisors may require that the candidate, in an early stage of the work, presents a written plan for the completion of the work.

The original contribution of the candidate and material taken from other sources shall be clearly defined. Work from other sources shall be properly referenced using an acknowledged referencing system.

The report shall be submitted in two copies:

- Signed by the candidate
- The text defining the scope included

- In bound volume(s)
- Drawings and/or computer prints which cannot be bound should be organized in a separate folder.

Ownership

NTNU has according to the present rules the ownership of the thesis. Any use of the thesis has to be approved by NTNU (or external partner when this applies). The department has the right to use the thesis as if the work was carried out by a NTNU employee, if nothing else has been agreed in advance.

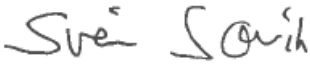
Thesis supervisors:

Prof. Svein Sævik, NTNU

Ph.D Hagbart Skage Alsos, Reinertsen

Deadline: June 10th , 2013

Trondheim, January , 2013


Svein Sævik
Trondheim, January , 2013

Preface

This thesis was developed and written during the spring semester 2013 at the department of Marine Technology at NTNU. The work presented is part of my Master of Technology degree at NTNU. The thesis is based on the work done during the fall semester 2012, with regards to the literature study and familiarization with the computer code SIMLA.

The main objective of the thesis was to perform dynamic studies on a pipe laying vessel, with a pipeline hanging over the stinger of the vessel, and calculating the fatigue life consumption at such a configuration over time. Several sea states was considered and analyzed to give grounds for a comparison between the states.

A CD is attached with the final document, which contains in addition to a digital copy of the thesis, all result- and input-files used in the various software programs.

My main supervisor for this thesis has been Svein Sævik at the department of Marine Technology at NTNU. He has helped me with everything from general writing tips to a better understanding of the physics behind the SIMLA software. His kind nature has always made it easy to ask for help.

In addition, the good people at Reinertsen AS, have been of great help during the birth of the thesis. Especially Hagbart Skage Alsos have been a great source of knowledge and general know-how. I look forward to any future collaboration.



Martin Suul

Trondheim, June, 2013

Summary

Sub-sea pipelines represent the most cost effective way of transporting oil & gas from the sub-sea field to the market. S-lay is the dominant installation method due to the horizontal firing line enabling several welding stations and efficient pipe string production. For S-lay, a stinger is used to support the pipe until it is lowered into the sea. For this method, pipeline installation is limited by the weather window and primarily due to the motions induced at the stinger tip by 1st order wave forces on the vessel. These motions will cause the pipeline to accumulate fatigue damage. This is especially the case when the lay vessel is forced to wait for whatever reason. The pipe will then have to be abandoned to avoid too much damage on the pipeline. The guideline for the allowed damage is no more than 10% of the total fatigue life, for the installation phase. This thesis will focus on the fatigue crack growth of the weld at the stinger tip section. And calculate the period of time it takes for the pipeline to reach the allowed damage criterion.

The analysis and calculations presented in this thesis will be based on the computer codes SIMLA and LINKpipe. A brief introduction to these codes will be presented. SIMLA will simulate the sea state and the vessel motion, to produce the cyclic bending stresses. These stresses are imported into LINKpipe, which will perform the fatigue calculations.

The sea states chosen for the analyses, were chosen based on the JONSWAP spectrum for the H_s chosen. The periods were chosen to give a wide view of how the fatigue would develop as the period changed

The fatigue crack growth after one hour of sea state and the number of hour to failure at the given sea state is given in the table below.

Analysis	H_s 1.5m					H_s 2.5m				
	T_p 5s	T_p 8s	T_p 9s	T_p 10s	T_p 13s	T_p 5s	T_p 8s	T_p 9s	T_p 10s	T_p 13s
Fatigue growth [mm]	0.00	0.00	0.00	0.01	0.02	0.00	0.00	0.02	0.05	0.10
Time to failure [h]	N/A ¹	9369	1403	476	197	N/A ¹	1089	261	103	48
10% of fatigue life [h]	N/A ¹	937	140	48	20	N/A ¹	109	26	10	5

The conclusion drawn from these results are that the fatigue life consumption is closely related to the RAO of the vessel. The method presented gives a good basis for the fatigue calculation of a pipeline being installed. The shortest time to failure was seen in the case of the 13 seconds period. This is consistent to the RAO of the vessel. The probability of a sea state of H_s 2.5 and T_p 13 seconds to be present is however quite small given the JONSWAP spectrum for these parameters.

¹ All stress range values lower than the threshold value for fatigue crack growth.

Infinite life is assumed

Sammendrag

Sub-sea rørledninger i dag den mest kostnadseffektive måten å transportere olje og gass fra feltet ut til markedet. S-lay er den dominerende metoden for å installere slike oljeledninger, på grunn av den effektive produksjons linja, som tillater flere sveisestasjoner. Ved denne metoden bruker man en ”stinger”, som er en støttekonstruksjon som henger ut fra fartøyet og som skal støtte rørledningen på vei ned i havet. Denne installasjonsmetoden er begrenset av været på grunn av de bevegelsene båten vil oppleve på grunn av bølgene. Disse bevegelsene vil påvirke rørledningen slik at den vil oppleve utmatting. Dette er spesielt viktig når fartøyet og produksjonen må vente. Dette kan gjøre at man blir nødt til å legge rørledningen ned på havbunnen for å hindre at utmattingen påvirker rørledningen for mye. Retningslinjene når det kommer til hvor mye utmattingskade man kan tillate er 10% av det totale utmattingslivet for installasjonsfasen. Denne avhandlingen vil fokusere på utmattingsprekkveksten i en sveis som blir stående påp stingertuppen, og beregne hvor lang tid det tar før rørledningen har nådd tillatt utmattingskade.

Analysene og beregningene presentert i denne avhandlingen er basert på dataprogrammene SIMLA og LINKpipe. En kort introduksjon i disse programmene vil bli presentert. SIMLA simulerer sjøtilstandene og bevegelsene på fartøyet for å beregne de sykliske spenningene som påvirker rørledningen. Disse syklene og tilhørende spenningsvidder importeres inn i LINKpipe, som beregner utmattingen.

Sjøtilstandene som er valgt i denne avhandlingen er basert på JONSWAP spekteret for den valgte H_s verdien. Periodene som ble valgt er valgt for å gi et bilde av hvordan utmattingen vil utvikle seg ettersom perioden endrer seg.

Utmattingsprekkveksten etter en times sjøtilstand, og antall timer til brudd for de ulike sjøtilstandene er gitt i tabellen under.

Analyse	H _s 1.5m					H _s 2.5m				
	T _p 5s	T _p 8s	T _p 9s	T _p 10s	T _p 13s	T _p 5s	T _p 8s	T _p 9s	T _p 10s	T _p 13s
Utmattingssprekkvekst [mm]	0.00	0.00	0.00	0.01	0.02	0.00	0.00	0.02	0.05	0.10
Tid til brudd [h]	N/A ²	9369	1403	476	197	N/A ¹	1089	261	103	48
10% av utmattingstid [h]	N/A ¹	937	140	48	20	N/A ¹	109	26	10	5

Konklusjonen som kan dras fra disse resultatene er at utmattingsskaden som rørledningen tar er veldig knyttet opp mot fartøyets RAO. Metoden presentert i avhandlingen gir en god base for å beregne utmattingen på en rørledning under installasjon. Den korteste tiden til brudd ble sett på sjøtilstandene med 13 sekunders periode, som er forventet ut i fra fartøyets RAO. Sannsynligheten for en sjøtilstand med H_s 2.5 m og en periode på 13 sekunder er derimot ganske liten gitt JONSWAP spekterets fordeling.

² Spenningsvidden er under grenseverdien for utmattingssprekkvekst. Derfor antas ingen sprekkvekst.

Contents

1	INTRODUCTION.....	2
1.1	BACKGROUND	2
1.2	SCOPE OF THESIS.....	2
2	PIPELINES	4
2.1	INTRODUCTION.....	4
2.2	DESIGN STAGES.....	4
2.2.1	<i>Pipeline Design Analysis</i>	5
2.2.2	<i>Pipeline Routing</i>	6
2.2.3	<i>Intervention methods</i>	7
2.2.4	<i>Vortex Induced Vibrations</i>	8
3	INSTALLATION METHODS	11
3.1	S-LAY	12
3.2	J-LAY	14
3.3	REELING	15
3.4	LOADS AND FAILURE MODES.....	15
3.4.1	<i>Local buckling</i>	16
3.4.2	<i>Hydrodynamic forces</i>	17
4	ENVIRONMENTAL CONSIDERATIONS.....	19
4.1	WAVES	19
4.1.1	<i>Wave spectrums</i>	20
4.2	WIND	25
4.3	CURRENTS	25
5	FATIGUE, FRACTURE AND MATERIAL CONSIDERATIONS	26
5.1	FRACTURE CALCULATIONS.....	26
5.1.1	<i>Fracture Assessment</i>	28
5.2	FATIGUE	28
5.2.1	<i>SN-curve</i>	29
5.2.2	<i>The Mine Palmgren summation</i>	31
5.2.3	<i>Welded joints – Fatigue crack growth</i>	32
5.2.4	<i>Fatigue crack growth and inspection strategy</i>	33
5.3	NDT TESTING	34
5.4	MATERIAL PARAMETERS	35
5.4.1	<i>Fabrication considerations</i>	36

5.4.2	<i>Welding</i>	36
5.4.3	<i>Corrosion</i>	39
5.5	ENGINEERING CRITICALITY ASSESSMENT (ECA) (REINERTSEN, 2010).....	41
6	NONLINEAR FINITE ELEMENT METHOD	43
6.1	BASICS OF THE FINITE ELEMENT METHOD	43
6.1.1	<i>Equilibrium</i>	43
6.1.2	<i>Kinematic compatibility</i>	43
6.1.3	<i>Constitutive Equations</i>	44
6.2	TOTAL LAGRANGIAN (TL) AND THE UPDATED LAGRANGIAN (UL) FORMULATIONS 46	
6.3	DYNAMIC ANALYSIS	47
6.4	SOLUTION METHODS.....	48
6.5	PIPE ELEMENT	49
6.6	NONLINEARITIES	49
7	LINKPIPE	51
7.1	GENERALIZED DISPLACEMENTS AND INTERPOLATION FUNCTIONS	52
7.2	GENERALIZED FORCES	53
7.3	THE LINEAR ELASTIC LINE-SPRING.....	55
7.4	SOLUTION TECHNIQUES	59
8	SIMLA MODEL	60
8.1	MODEL BACKGROUND	60
8.2	WAVE DATA	62
8.3	SIMLA MODEL.....	63
8.3.1	<i>Critical Installation Phase</i>	64
9	RESULTS SIMLA	65
9.1	RAINFLOW COUNTING AND POST PROCESSING.....	65
10	LINKPIPE MODEL	66
10.1	ECA PARAMETERS.....	66
10.1.1	<i>Weld Flaw</i>	<i>Error! Bookmark not defined.</i>
10.1.2	<i>Correction factor</i>	66
11	RESULTS LINKPIPE	67
12	DISCUSSION, CONCLUSION AND FUTURE WORK	68
12.1	DISCUSSION.....	68
12.2	CONCLUSION	69

12.3	FUTURE WORK.....	69
13	APPENDIX.....	74
13.1	STRESS – TIME PLOTS FROM SIMLA	74

List of figures

FIGURE 1 VIBRATION TRAJECTORIES OF A FLEXIBLE BEAM	9
FIGURE 2: S-LAY CONFIGURATION (OFFSHORE ENGINEERING , 2012)	12
FIGURE 3: J-LAY CONFIGURATION (2B1ST CONSULTING, 2012).....	14
FIGURE 4: REEL LAY CONFIGURATION.....	15
FIGURE 5 IRREGULAR SEA BUILD UP (MOAN, 2004) (DEPARTMENT OF MARINE TECHNOLOGY)	20
FIGURE 6 WAVE ELEVATION REPRESENTED AS A GAUSSIAN DISTRIBUTION (DEPARTMENT OF MARINE TECHNOLOGY)	21
FIGURE 7 TIME SERIES AND FREQUENCY DOMAIN RELATION.....	22
FIGURE 8 JONSWAP SPECTRUM FOR $H_s = 4.0$ M, $T_p = 8.0$ S FOR $\gamma=1$, $\gamma=2$ AND $\gamma=5$. (DNV, 2010)	25
FIGURE 9: CYCLIC LOADING	29
FIGURE 10: EXAMPLE OF AN S-N CURVE	30
FIGURE 11 MINER PALMGREN PROCEDURE FOR VARIABLE LOADING	31
FIGURE 12: CRACK GROWTH RATE CURVE (CAMBRIDGE - MIT, 2012)	32
FIGURE 13 HEAT AFFECTED ZONE AND GRAIN GROWTH.....	37
FIGURE 14: KINEMATIC AND ISOTOPIC HARDENING A UNI-AXIAL CASE (SÆVIK, 2012)	45
FIGURE 15 TYPICAL MESH IN LINKPIPE.....	51
FIGURE 16 LINE-SPRING ELEMENT	52
FIGURE 17 JONSWAP SPECTRUM AND PITCH AND HEAVE RAOs. THE RAOs REMAIN DIMENSIONLESS FOR THE PRESENTATION PURPOSE.....	63
FIGURE 18 STRESS-TIME PLOT AT THE STINGER TIP.....	64
FIGURE 19 H_s 1.5M T_p 5S.....	74
FIGURE 20 H_s 1.5M T_p 8S.....	75
FIGURE 21 H_s 2.5M T_p 8S.....	75
FIGURE 22 H_s 1.5M T_p 9S.....	76
FIGURE 23 H_s 2.5M T_p 9S	76
FIGURE 24 H_s 1.5M T_p 10S.....	77
FIGURE 25 H_s 2.5M T_p 10S.....	77
FIGURE 26 H_s 1.5M T_p 13S.....	78
FIGURE 27 H_s 2.5M T_p 13S.....	78

List of tables

TABLE 1 SIMPLIFIED LAY CRITERION, OVERBEND.....	17
TABLE 2 PIPE MATERIAL DATA.....	60
TABLE 3 PIPE CHARACTERISTICS.....	61
TABLE 4 TENSION PARAMETERS.....	62
TABLE 5 ANALYSIS MATRIX.....	62
TABLE 6 RESULTS LINKPIPE.....	67

1 Introduction

1.1 Background

Sub-sea pipelines represent the most cost effective way of transporting oil & gas from the sub-sea field to the market. A large network of subsea pipelines has therefore been installed both at the Norwegian continental shelf and elsewhere. The development of the installation methods used for offshore pipeline installation has become more and more important over the last years. Longer and deeper installation projects have become increasingly common, as the search for oil and gas has taken us to harder to reach places on the seabed.

For large diameter pipelines (>16") S-lay is the dominant installation method. The horizontal firing line enables several welding stations and efficient pipe string production. For S-lay, a stinger is used to support the pipe until it is lowered into the sea. For this method, pipeline installation is limited by the weather window and primarily due to the motions induced at the stinger tip by 1st order wave forces on the vessel. At a certain sea state the associated cyclic loads may cause fatigue fracture in the weld positioned at the stinger tip. This is specially the case if the installation process is stopped for some reason, so that the same pipe section is exposed to many cycles. For certain sea states the pipeline may even have to be abandoned and laid onto the seabed for later recovery when the sea state allows continued installation.

1.2 Scope of Thesis

The DNV-OS-F101 states that the consumption of fatigue life of a pipeline during installation should be under 10% of the total fatigue life. This thesis will use the computer code SIMLA to investigate the dynamic forces on the pipeline. These forces will be subjected to a fatigue analysis using another computer code, LINKpipe, to investigate the consumption of fatigue life during installation in different sea states. The basis of the analysis is taken from the Ormen Lange project, using the 16" pipeline installed at a depth of 880 m.

The software simulated an hour of sea. This was assumed to capture the necessary amount of data regarding the dynamics of the pipeline catenary. In order to estimate the time to failure of the pipeline, this hour was multiplied with the desired number of

hours. This approach was selected to make the analysis time more manageable. The disadvantage of this approach is that the statistical distribution of the waves may be off. However, it is assumed that one hour was sufficient.

The dynamic input to LINKpipe will be from the computer code SIMLA. The simulation models have their basis in a comparison model comparing SIMLA to another pipeline computer code, OFFPIPE. Professor Svein Sævik at MARINTEK in Trondheim developed the model used in this thesis. This model has been modified to suit the fatigue assessment to be performed.

The most exposed point along the pipeline catenary will be at the tip of the stinger. The stinger tip will be the point at which the cyclic loading of the pipeline has the largest stress ranges. This point will be the focus of this thesis, as it will represent a worst-case scenario of a weld being held here for an extended period of time. However, a general description of other points of interests will be given. Such points are for instance the touchdown point and in the sagbend section of the catenary.

The stress ranges is a key parameter in the fatigue analysis. The stress the pipeline is subjected to is well within the elastic area of the material, and will by itself not cause any damage to the pipe. It is however, the combination of the stress range value and the number of cycles the pipeline goes through, which will in time cause damage to the pipeline.

2 Pipelines

2.1 Introduction

Many aspects have to be accounted for when installing a pipeline and the procedure for doing so is a meticulous undertaking. The different pipelines can be divided into two main categories, trunklines and flowlines.

The flowline is a transportation line within the field. Usually connected to the wellhead through a manifold or to production facilities such as heaters or separators. (Schlumberger, 2012) These lines are exposed to non-refined fluids and must endure a high corrosive environment, which requires them to be designed to withstand quite harsh conditions. They can also be used to transport secondary fluids within the field, such as water or gas to be injected back into the well. The flowline is usually a larger diameter pipe, but the sizing ranges from 2” to 12” diameters, both single-bore and multi-bore.

A trunkline is an export pipeline, which exports oil or gas from the field to shore. The transported medium has been refined and handled by the systems on the platform or FPSO, so the corrosivity of the pipe content has been greatly reduced. The temperature, pressure and corrosivity are tailored for the pipe transport.

2.2 Design Stages

The design of pipelines is usually performed in three stages:

- Conceptual engineering
- Preliminary engineering
- Detail engineering

The objectives of each of these steps are case specific, but the main objectives are generally as follows.

Conceptual engineering where, the technical feasibility and constraints of the project are established, limiting the non-viable options. Information concerning forthcoming design and construction are considered, which will include the interface with existing or planned systems. A basic understanding and estimation of cost and scheduling are

also performed. The basic idea of the concept study is to reveal difficulties and areas of concern.

Primary objectives for the preliminary engineering are to perform the pipeline design so that the system concept is fixed. This includes the sizing of the pipeline, wall thickness and pipeline material grade. This is then verified against the code requirements for installation, commissioning and operation of the pipeline. A material take-off sufficient to order the linepipe should be performed. The linepipe may have a long delivery time, and will therefore need to be ordered at an early stage. At this stage the necessary applications to the authorities are prepared.

The detail design of a project is to finalize the design and prepare the detailed documentation required for procurement, prefabrication and installation. This includes routing optimization, detailed pipeline design including wall thickness and coatings, vortex induced vibration (VIV), on-bottom-stability, global buckling and installation considerations, updating alignment sheets to comply with the latest surveys, specification of covering materials, cost applications construction activities such as pipelay, survey, welding, subsea tie-ins and subsea structure installation, and commissioning of the pipeline. The finalized material take-off (MTO) is also prepared and preparing the finalized design information to the certification authorities. (Bai & Bai, 2005)

2.2.1 Pipeline Design Analysis

A series of codes and standards governs the stresses and strains a pipeline is exposed to. To determine if these stresses are acceptable, a series of analysis are performed. Analyses are performed to ensure that the stresses the pipeline is subjected to is within the standard requirements. These analyses encompass several different aspects, some of which are, hoop stress, longitudinal stress, equivalent stress, pipeline stability, expansion, buckling and free spans. The first three stages are directly related to the wall thickness sizing of the pipeline. These steps should be performed in conjunction with hydrostatic collapse or buckle propagation analysis from the installation analysis.

The hoop stress is governed by the following equation

Equation 1

$$\sigma_h = (p_i - p_e) \frac{D - t}{2t}$$

where σ_h is the hoop stress, p is the internal or external pressure, D is the outside diameter of the pipeline and t corresponds to the minimum wall thickness of the pipeline. Some variations concerning the hoop stress limit exist, but all relates to a certain fraction of the specified minimum yield stress (SMYS). This fraction is regarded as a safety factor.

The longitudinal stress is the axial stress experienced by the pipe wall. The stress consists of contributions from bending, hoop, thermal and end-cap force induced stress, and can be calculated as

Equation 2

$$\sigma_l = 0.3\sigma_{lh} + \sigma_{lb} + \sigma_{lt} + \sigma_{lc}$$

where σ_l is the longitudinal stress, σ_{lh} is the hoop stress, σ_{lt} is the thermal stress and σ_{lc} is the end-cap stress. Using a consistent sign system is imperative when employing this equation. Here, tensile stress is regarded as a positive value.

The combined stress is determined differently depending on the different standards and codes that are used for the project. However, the equivalent stress can usually be expressed as

Equation 3

$$\sigma_e = \sqrt{\sigma_h^2 + \sigma_l^2 - \sigma_h \sigma_l + 3\tau_{lh}^2}$$

where σ_h and σ_l is the hoop and longitudinal stress respectively and τ_{lh} is the tangential shear stress. (Bai & Bai, 2005)

2.2.2 Pipeline Routing

The straightest line is usually the shortest, and will therefore be the most economic. However, the seabed is not a plane surface. This may cause the pipeline to have to cross unfavorable areas such as landfall sites, larger depths or span valleys. Such areas along the straight path between two terminal points may require an alternative

route selection. The final route selection is a significant part in the final cost of an installation project, affecting the length of the pipeline and the interventions to be done along the route. Careful surveys are done to investigate different route options to ensure the optimal route is chosen. A route design should be performed to minimize pipeline length, avoid requirement of presweeping, avoid or minimize pre- and post-lay free span supports and to minimize the trenching or rock dumping to be done. In general, minimize the amount of extra work to be done to ensure the integrity of the pipeline. Some intervention methods will be discussed further in a later section.

The route options are investigated by surveys to determine the topography of the seabed. This can be done by an autonomous underwater vehicle, or AUV, equipped with mapping instruments. The data is stored as a survey file, easily processed or imported into several computer codes, which allows for easy and graphical assessment.

When the topography of the seabed indicates that the pipeline requires special considerations, the pipeline must be investigated against applicable standards and requirements to ensure that excessive yielding, fatigue, vortex induced vibrations (VIV) and interference are controlled. These modes will control the allowable span length according to current conditions and fishing activity in the area. If the span in question should cause the span to exceed the allowable limits, necessary measures need to be taken to prevent this. The flow of current will cause vortex shedding around a pipeline. VIV will be discussed in a later section.

2.2.3 Intervention methods

The different intervention methods described briefly above, consist of manipulating the seabed in such a way to reduce the stresses the pipeline is subjected to. The idea behind these methods is usually quite simple, but the location of the areas in question may leave the process quite complicated. The most common intervention methods are installation of free span supports (rockdumping), trenching, and burying. The installation of free span supports are basically the elimination of small valleys and gorges in the seabed, reducing the free spanning length of the pipeline. This will reduce the potential for VIV, and therefore reduce fatigue exposure of the pipeline.

Trenching is a procedure in which a trench is dug to either bury the pipeline or to ease the stress concentrations in relation to peaks on the seabed. In the latter case, the peak is rounded out to a smoother transition. When the pipeline is buried, it is concealed from the currents and restrained with regards to lateral buckling. Rock dumps can be used to fix the pipeline axially. This is done to control the expansion of the pipeline by allowing the pipeline to buckle laterally a defined geometry.. Rock dumps may also be utilized in relation to free spans to prevent pipeline expansion to feed in into the span, causing the pipeline to sag.

2.2.4 Vortex Induced Vibrations

A design parameter that needs to be accounted for when encountering free spans along the pipeline route, is the vortex induced vibrations (VIV) that occurs when slender structures are exposed to currents. The vibrations are caused by the vortices that are shed from top and bottom of the pipeline, causing it to oscillate. The forces developed are defined by the direction of the incoming undisturbed current flow, where the two are called in-line (IL) or cross-flow (CF). The load frequency of the CF force will have the same frequency as the vortex shedding, where at least two vortices are shed per cycle, and the IL force will have twice this frequency. Traditionally, the CF response has been the governing parameter due to its larger amplitude, but in later years the effect of the IL response has also been taken into consideration.

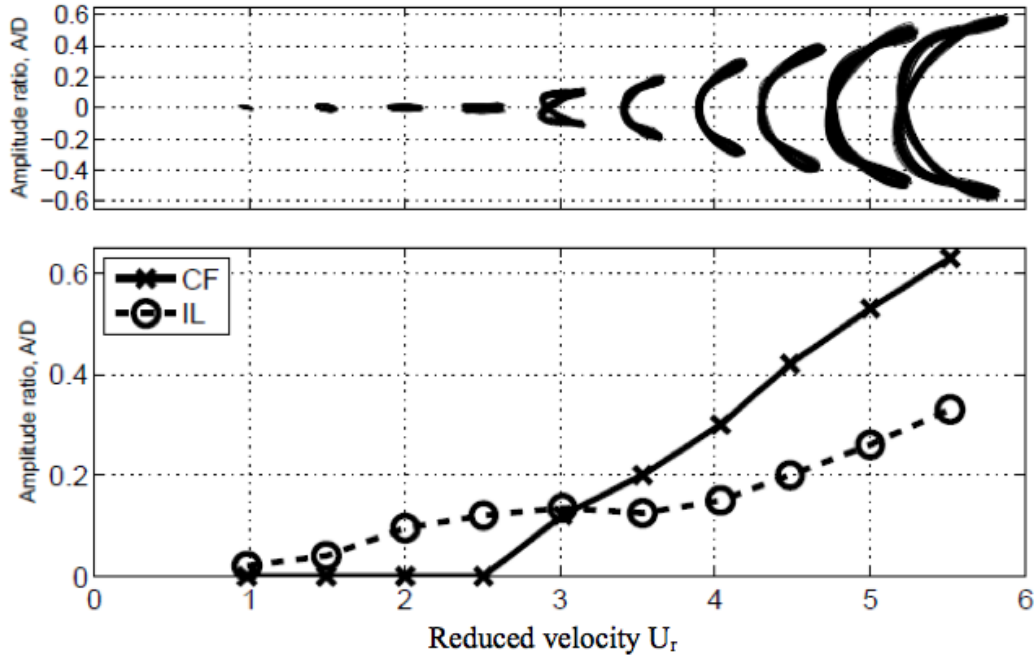


Figure 1 Vibration trajectories of a flexible beam

As seen in Figure 1 Vibration trajectories of a flexible beam, VIV is a vibration that will increase with the increasing current velocity and the shedding frequency. For a slender structure with identical eigenfrequencies in both CF and IL direction, it will therefore experience IL response at a lower current velocity than CF. The current velocity in Figure 1 Vibration trajectories of a flexible beam is given as reduced velocity, which is given by

Equation 4

$$U_R = \frac{U}{Df_0}$$

From the figure it is seen that the IL response will start at a reduced velocity just above 1.0 and the CF response at 2.5.

As the Strouhal number is close to 0.2 for the Reynolds number range, a common criterion for CF VIV is

$$U \geq 5Df_0$$

However, this equation yields an approximate value for the fully developed cross-flow vibration. As seen in Figure 1 Vibration trajectories of a flexible beam CF VIV may occur at lower current speeds.

The VIV is usually considered a self-limiting response. This is due to its dependency on the response amplitude. If the amplitude exceeds a certain limit the vortex shedding will not be able to transfer energy from the current flow to the structure. It will rather limit the amplitude as the shedding process will occur out of phase with the response amplitude and therefore lead to damping of the VIV response. This is however not valid for non-circular cross sections, where a galloping of the VIV response has been experienced in tests.

The cyclic nature of the VIV response leads to an accumulation of fatigue damage. It will also result in an increase of drag on the pipeline. The increased drag will result in an increase of the static loading and deformation of the pipeline. It is however the fatigue aspect of VIV which is the most common design criteria when it comes to pipeline design. Several codes and regulations consider this aspect, but this alone is not enough to use as general guidelines. Hence, case specific assessments and calculations are needed to ensure the quality of the design. This is usually done by computer programs based on either a combination of computational fluid dynamics (CFD) and a FEM model, or an empirical model for hydrodynamic forces and a FEM model.

3 Installation methods

The selection of installation method is greatly dependant of the parameters imposed by the project, whether this is economical, design or installation practicality. Larger diameter pipe may have to be installed by a certain method, while small flowlines is more effectively installed by another method. The economical issue is often decided by the cost of the installation vessel. As some installation vessels run at high daily rates, the time required for installation will affect the total cost. In addition, the routing of the pipeline and the waterdepth may impose requirements with regards to the installation vessel maneuverability. All these parameters influence the choice of installation method.

Three main installation methods are in use:

- S-lay
- J-lay
- Reeling

3.1 S-lay

The most common way of installing subsea pipelines of diameters above 16" is the S-lay method. The method is concentrated around a vessel, which can be compared to a floating pipeline factory. This factory includes storage facilities for 12m pipe joints, welding stations, NDT testing facilities and coating stations. The main production line, or firing line, includes several welding stations for double joints, NDT station and multiple coating stations, where the pipe lengths are welded together to form the pipeline. The linepipe is usually manufactured in 12 m lengths and are often welded together to 24 m lengths before entering the firing line. The welding can be done in several ways, which is described later in the thesis. The welded pipeline passes through several stations for NDT, which can include both X-ray and ultrasonic testing of the welds. These methods and stations are also described later in the thesis.

The vessel is maneuvered by dynamic positioning (DP) or anchor pulling, and is moved at intervals corresponding to the pipe lengths finished by the firing line.

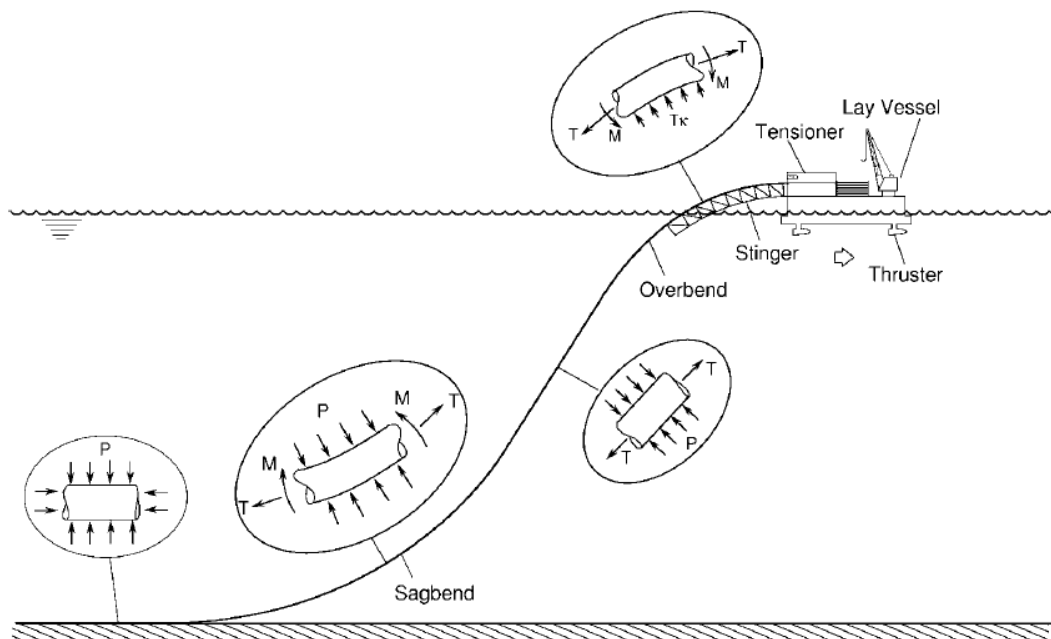


Figure 2: S-lay Configuration (Offshore Engineering , 2012)

After the firing line, the pipeline passes through a tensioner. The tensioner applies the axial tension required for the pipeline to assume an S-shaped catenary configuration to the seabed. The stinger, which is located behind the tensioner, is a support structure which controls the pipeline curvature as it enters the sea. The stinger is a frame structure, with rollers acting as supporting points along the stinger. The point where

the pipeline leaves the stinger is called the departure point. The departure angle of the stinger is an important parameter dependent of the catenary configuration and the size of the unsuspended span. This angle is dependent on the tension applied, the weight of the pipe and the water depth. The stinger configuration and the tension applied must be such that the pipe never touches the steepest point, or the last roller, of the stinger. This may cause an area of high bending stress that may cause buckling of the pipeline.

The tension applied to the pipeline will also define the radius of the sagbend. The sagbend is where the pipeline starts to curve back to a horizontal configuration. A low tension, will cause this curvature to be very steep and a local buckling may occur.

For shallow water installation, the weight of the free spanning pipe is partly carried by membrane and beam bending stiffness effects. For deeper water, membrane effects will mainly take the load. The bending stiffness will contribute to a reduction in the applied horizontal tension force during shallow water installation.

Pipeline fatigue is also an issue to be considered for S-lay installation. The pipeline is subjected to fatigue inducing motions at the stinger tip as a result of the dynamic motions of the vessel. Here the interaction between the stinger and the pipeline may restrict the weather window of installation.

This thesis will use the S-lay model in the further analysis of pipeline fatigue.

3.2 J-Lay

For a J-lay configuration the pipeline is installed in a J-shaped catenary. The angle the pipeline enters the water is governed by the water depth, the weight of the pipe and the horizontal tension. The buckling capacity of the pipe governs the minimum curvature in the sagbend, and this again is controlled by the amount of tension applied to the pipeline. A low tension will provide a high entry angle and a short layback length. These parameters all determine the horizontal tension needed to keep the shape of the catenary down to the seabed. The J-lay method can be done by either reeling or by welding pipe lengths on the vessel. The reeling part of the J-lay method is by some considered a separate method for installation and will be discussed later.

The weld approach has some unique challenges. The setup is compiled of a high tower, which the pipe is launched from. The advantage is that the bending moment at the surface (overbend) is eliminated. The challenge is that the welding and NDT of the final field joint has to be done in the high tower at a near vertical angle. There will also only be room for one welding station in the tower, which reduces the lay rate of the method. The method is mainly used for deep-water installation of large diameter pipes.

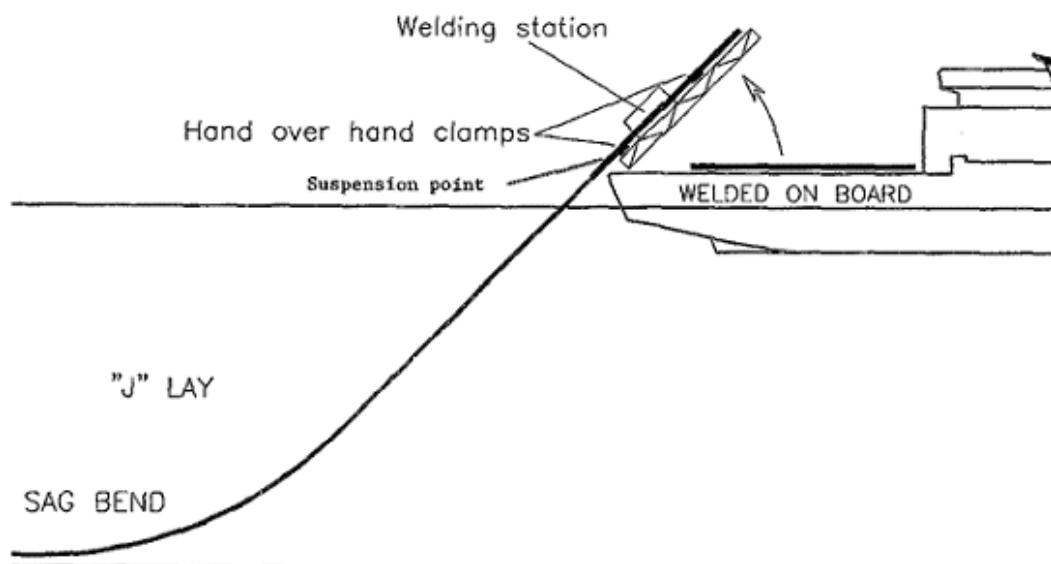


Figure 3: J-Lay Configuration (2B1st Consulting, 2012)

3.3 Reeling

The reeling method is based on the same principles as the J-lay method. Except the pipe is fabricated and welded onshore, reeled onto a large reel, which in turn is transported out to the installation location and then installed by unreeling the reel.

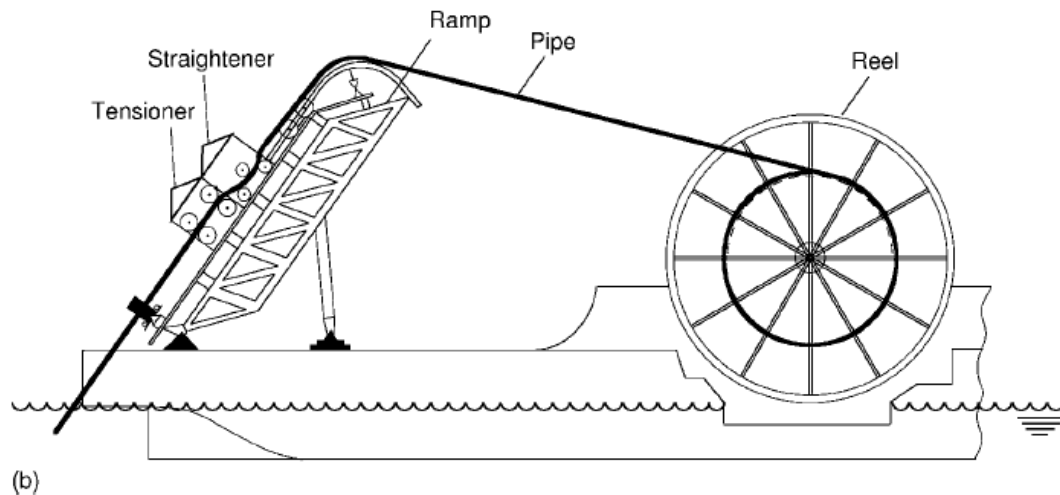


Figure 4: Reel Lay Configuration

After unreeling of the pipe, it is sent across an aligner and through a straightener. This straightens the pipe, which is needed due to the small deformation obtained in the reeling process. The reeling method is limited to 18" due to the large bending moment achieved in the reel. This can cause collapse of the cross section if larger diameters are utilized. The method can achieve a high lay rate due to the lack of welding and NDT procedures on-site.

Other special methods exist, such as several tow methods. These are however usually used for shorter lengths, and will not be discussed further in this thesis.

3.4 Loads and failure modes

Depending on the installation method used, the pipeline will experience loads from the lay-vessel and the sea. These loads are hydrostatic pressure, tension and bending. The degree of these loads will vary with the installation method used. Minimum lay tension is estimated during the design phase, according to a given stinger radius or curvature. This is to ensure that the load effects are within the strength criteria of the pipeline. This is usually done with finite element model, using computer tools. The static configuration of the pipeline catenary is governed by

- Tension at the lay-vessel
- Curvature of the stinger
- Roller positions
- Departure angle
- Weight of the pipe
- Pipe bending stiffness
- Water depth

It is especially the curvature over the stinger and in the sagbend, which is critical. Here, collapse of the cross section is likely to occur if the required configuration is not achieved. The sagbend curvature is governed by the applied tension, which will limit the curvature of the sagbend by stretching it out.

As the pipeline is lowered down into the sea, the hydrostatic pressure will increase with water depth. For the installation phase, the pipeline has no internal pressure. This will affect the response of the pipeline catenary, as the radial pressure will induce an axial strain via the Poisson's effect. This will alter the stiffening of the pipeline from the tension applied, which in turn will affect the curvature of the pipeline.

The stinger will support the overbend part of the catenary. This will limit the curvature and bending moments experienced by the pipeline. However, stress concentrations may occur at the roller locations, where the pipeline is in contact with the stinger. Careful considerations during the modeling of the stinger should be taken, to represent this accurately.

3.4.1 Local buckling

Local buckling can occur in the pipeline when it is subjected to external pressure, longitudinal force and bending. The failure mode can cause yielding of the cross section or buckling on the compressive side of the pipe. Several guidelines and recommendations for local buckling analysis exist. DNV gives a simplified laying criterion in regards to the local buckling failure mode in both the overbend and the sagbend of the catenary (DNV, 2010). For the overbend, the static loading of the pipeline shall not exceed the values given in the following table. The table gives reference to some of the more common grades of steel used for pipelines. The X65 grade steel is used in the model used in this thesis. These values include effects of

bending, axial force and local roller loads, while stress concentration factors do not need to be included for criterion I.

Table 1 Simplified lay criterion, overbend

Criterion	Material quality			
	X70	X65	X60	X52
I	0.270%	0.250%	0.230%	0.205
II	0.325%	0.305%	0.290%	0.260%

Criterion II considers static plus dynamic loading. Here, all effects including stress concentration or varying stiffness shall be included.

For the sagbend, a different criterion applies. This criterion is for the combined static and dynamic loading scenario, stating that the equivalent stress in the sagbend and at the stinger tip shall be less than

Equation 5

$$\sigma_{eq} < 0.87f_y$$

where f_y is equivalent to the SMYS of the material. When utilizing this equation, all load effect factors are set to a unity value.

3.4.2 Hydrodynamic forces

The hydrodynamic forces related to a pipeline installation case are drag and inertia forces that act on the pipe cross section. These forces can oscillate and cause transverse displacement of the catenary. The forces in question come from the particle velocity of the wave. This depends on the wave height, water depth and wave period. The wave velocity potential is given as

Equation 6

$$\varphi = \frac{g\zeta_a}{\omega} e^{kz} \cos(\omega t - kx)$$

for infinite water depth. The velocity potential decreases exponentially with the e^{-kz} component. So it is easily seen that the wave will affect the pipeline more at the surface than lower on the catenary (Faltinsen, 1990).

The drag force developed at a circular structure is given by:

Equation 7

$$F_D = \frac{1}{2} \rho C_D (U + V)^2$$

where F_D is the drag force per unit length, ρ is the density of the water, C_D is the drag coefficient of the structure, D is the diameter of the structure, U is the particle velocity and V is the current velocity.

The inertia forces due to the particle acceleration is given by

Equation 8

$$F_I = \rho C_M \frac{\pi}{4} D^2 a$$

where F_I is the inertia force per unit length, ρ is the density of the water, C_M is the drag coefficient of the structure, D is the diameter of the structure and a is the particle acceleration component. The total force is then given by the Morison equation, where drag and inertia forces are combined.

Equation 9

$$F = F_D + F_I = \frac{1}{2} \rho C_D (U + V)^2 + \rho C_M \frac{\pi}{4} D^2 a$$

The coefficients given in the mentioned equations are empirically determined and are represented as a function of several parameters i.e. Reynolds number and Keulegan-Carpenter number.

4 Environmental Considerations

4.1 Waves

Ocean waves are irregular by nature. This means that the sea state consists of a random collection of waves acting in different directions and has altogether different characteristics. A random wave model best describes such a sea state. A random wave model may be set up in two different ways: A linear- and a non-linear way. A linear model will consist of the sum of many small linear wave components with different amplitude, frequency and directions. The phases between the waves are random in respect to each other. A non-linear wave model allows for sum- and difference frequency wave components caused by non-linear interaction between the individual wave-components.

The wave conditions used for structural analysis may be described by deterministic design wave methods or by stochastic methods, where a wave spectrum is applied. For structures with a significant dynamic response, the stochastic approach is used to model the surface and its kinematics by time series.

A sea state is specified by a wave frequency spectrum with a given significant wave height, a representative frequency, a mean propagation direction and a spreading function. In applications the sea state is usually assumed to be a stationary random process, where three hours has been introduced as a standard time between registrations of sea states when measuring waves. However, any period between 30 minutes to 10 hours may occur.

The general characteristics of a wave are given by a series of different parameters, usually referenced to a regular traveling wave, propagating with a permanent form. The *wave length* (λ) of such a wave is the distance between two successive wave crests. The *wave period* (T) represents the time interval between two successive wave crests passing a particular point. The *phase velocity* ($c=\lambda/T$) or the propagation velocity of a wave, *wave frequency* ($f=1/T$), *wave angular frequency* ($\omega=2\pi/T$) and *wave number* ($k=2\pi/\lambda$) are also specific wave parameters included in the sea state considerations. In addition to these, the surface conditions are described by several wave parameters such as the surface elevation during a wave, which describes the

distance between the still water and the wave surface. Wave crest height and wave trough depth are the distance from the still water to the crest and trough of the wave. These two parameters represent the total wave height of the wave. All of these parameters give grounds for the different analytic wave theories, which relate the parameters to each other to give the motion of the water particle throughout the flow of the wave. In order to relate this motion to the depth of the water column, the dispersion relation is utilized. This relationship can analyze the water column for finite and infinite water depths. (DNV, 2010)

The nonlinear waves are considered asymmetric, where the wave crest height is considered to be larger than the wave trough depth. Nonlinear waves are also subject to different energy considerations, where the average energy density is given by the sum of the average kinetic and potential wave energy per unit of horizontal area (E). This, in addition to the energy flux of the wave, which is the average transfer rate of energy per width unit of the wave (P), gives the group velocity, $c_g=P/E$, which yields the wave energy transfer rate. (DNV, 2010)

4.1.1 Wave spectrums

A common way to describe the wave elevation ζ , is by summing all the wave components from waves which are propagating along the x-axis. (Faltinsen, 1990)

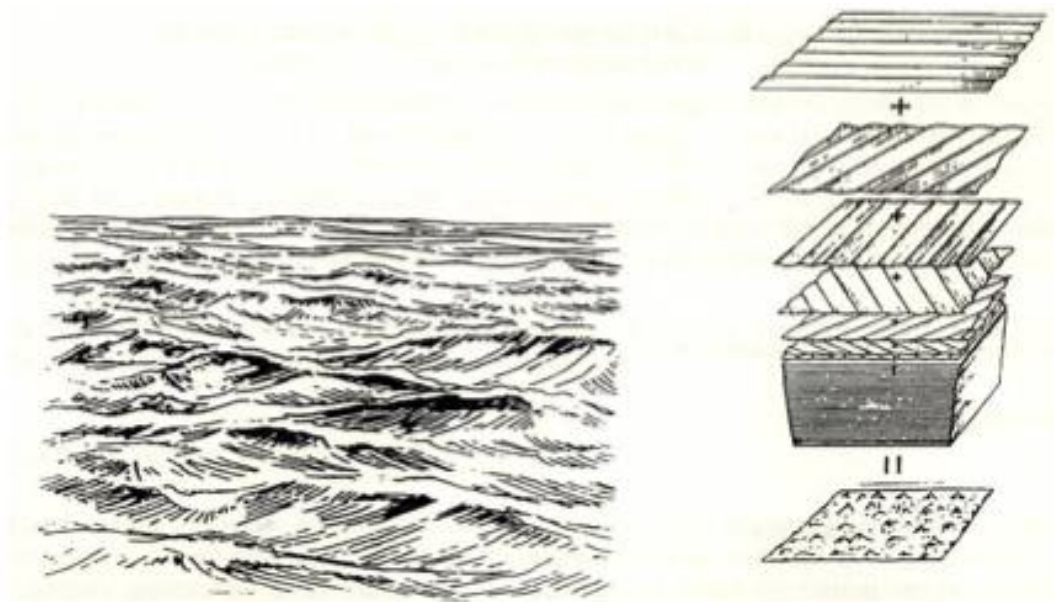


Figure 5 Irregular sea build up (Moan, 2004) (Department of Marine Technology)

The summation of the different wave elevations is given by:

Equation 10

$$\zeta(x, t) = \sum_{j=1}^{\infty} \zeta_{A_j} \sin(\omega_j t - k_j x + \varepsilon_j)$$

Where ζ_{A_j} represents the amplitude of a specific wave number j , while ω_j , k_j and ε_j represents the circular frequency, the wave number and the phase angle between the waves. The summation of the different irregular waves is then transformed to a sum of regular waves, easily represented by a Gaussian distribution. (Faltinsen, 1990)

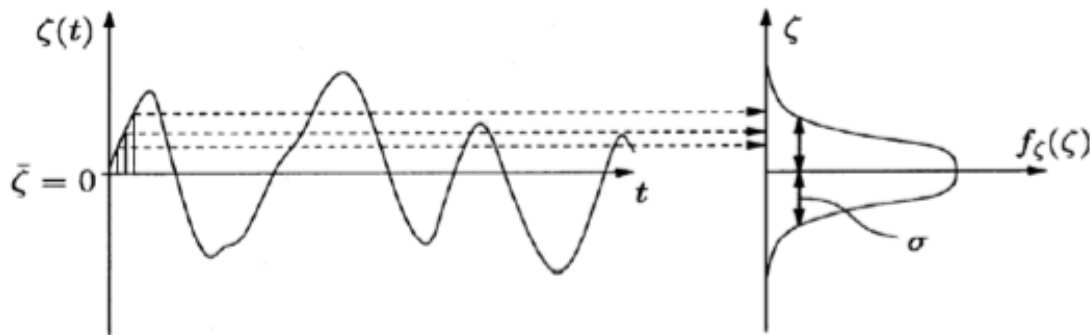


Figure 6 Wave elevation represented as a Gaussian distribution (Department of Marine Technology)

By introducing such a wave spectrum, we can transform the wave process from the time domain to the frequency domain. The relationship between wave amplitude and the frequency wave spectrum is given by:

Equation 11

$$\frac{1}{2} \zeta_{A_j}^2 = S_{\zeta}(\omega_j) \Delta\omega$$

where $\Delta\omega$ is the actual frequency interval. This equation can easily be combined with the summation formula for the different wave elevations:

Equation 12

$$\zeta(x, t) = \sum_{j=1}^{\infty} \sqrt{2S_{\zeta}(\omega_j) \Delta\omega} \sin(\omega_j t - k_j x + \varepsilon_j)$$

this spectral representation is a better way to express the wave elevation, due to its lesser storage space consumption. Such a spectrum may also be combined with transfer functions to produce other spectrums. This is some of the reasons the

frequency domain is usually used for analyzing the behavior of irregular sea.
(Faltinsen, 1990)

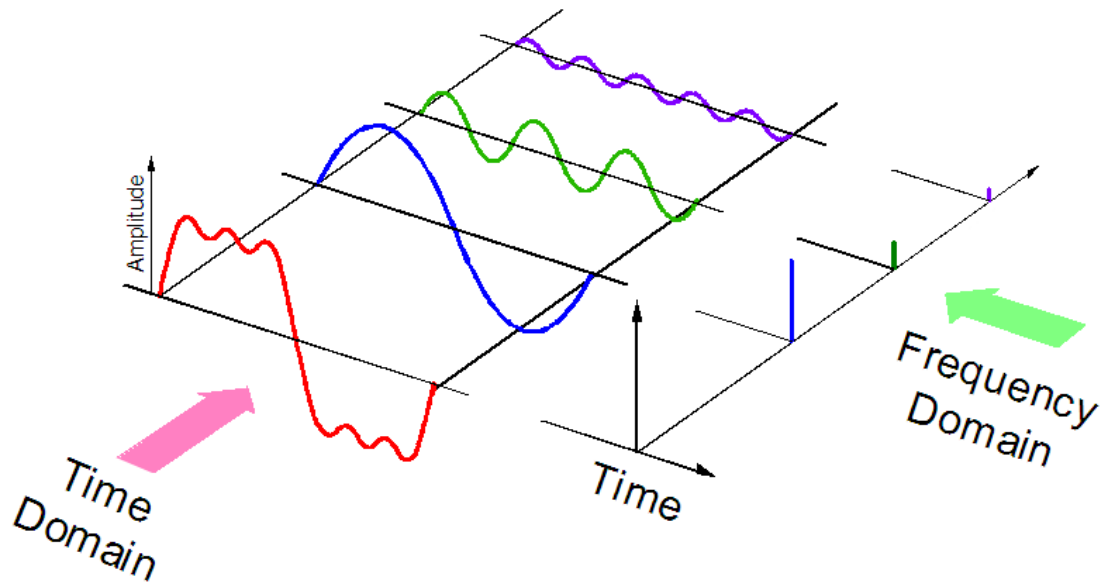


Figure 7 Time series and frequency domain relation

Applying the central limit theorem to equation 5.1 can easily show a Gaussian distributed wave elevation. This yields a mean value for the surface level and a variance (σ_ζ^2), which can be formulated as follows. (Larsen, 2009)

Equation 13

$$\sigma_\zeta^2 = \sum_{j=1}^{\infty} \frac{1}{2} \zeta_{A_j}^2 = \int_0^{\infty} S_\zeta(\omega) d\omega$$

The formula is formulated to show the wave spectrum and will contain all the statistical properties of ζ . The wave process may be evaluated by analyzing the time series in either a direct manner, or by utilizing a specified or standardized spectrum. This will allow for easy evaluation of the spectral moments and relating them to key parameters such as significant wave height. The moments are found by a general formula, given below. (Larsen, 2009)

Equation 14

$$m_0 = \int_0^{\infty} \omega^n S_\zeta(\omega) d\omega$$

from this equation it is easily seen that m_0 represents the variation of the wave elevation process.

The parameter significant wave height has been mentioned above. This parameter is a key parameter when it comes to evaluation a sea state. It represents the mean value of the 3rd highest waves in the sea state. This value is often referred to in weather forecasts, especially when describing extreme conditions. $H_{1/3}$ is the directly measured value of the wave heights from real samples, while an approximation of the significant wave heights may be calculated from the spectral moment, H_{m0} . When a spectrum fits the actual sea conditions in an area, the values for H_{m0} and $H_{1/3}$ will be almost identical. A frequently used approximation of H_{m0} is given below. (Myrhaug, 2007)

Equation 15

$$H_{m_0} = 4\sqrt{m_0}$$

The bandwidth of the wave process gives a perspective when it comes to evaluating the range of values in a wave spectrum. Broad banded spectrums have a larger range of different values, while the narrow banded spectrum consists of wave periods within a certain range of values. It is the wave periods of the waves within the spectrum that will decide whether or not the spectrum is broad- or narrow banded. This is easily investigated by comparing calculations from the spectral moments. (Myrhaug, 2007)

Equation 16

$$T_{01} = 2\pi \left(\frac{m_0}{m_1} \right), \quad T_{01} = 2\pi \left(\frac{m_0}{m_1} \right)^{\frac{1}{2}}, \quad etc$$

The bandwidth of the spectrum is decided by the difference between T_{01} and T_{02} . A small difference implies a narrow banded spectrum, while a larger difference implies a broad banded spectrum.

Two main spectrums are usually used for the analysis of marine structures, the Pierson-Moskowitz (PM) and the JONSWAP spectrums. These have different characteristics and usages. The PM spectrum is used for short-term analysis, as it will cover a time window of about three hours. The formulation of the spectrum is given by the equation below.

Equation 17

$$S_{PM}(\omega) = \frac{5}{16} H_s^2 \omega_p^4 \omega^{-5} \exp\left(-\frac{5}{4} \left(\frac{\omega}{\omega_p}\right)^4\right)$$

where $\omega_p = 2\pi/T_p$ is the angular spectral peak frequency, while H_s is the significant wave height.

The JONSWAP spectrum is a modification of the PM spectrum, which will include the characteristics of a developing sea state in a fetch limited situation. This will expand the time window of the spectrum, to allow for longer analysis. The JONSWAP spectrum is given by the equation below.

Equation 18

$$S_J(\omega) = A_\gamma S_{PM}(\omega) \gamma^{\exp\left(-0.5\left(\frac{\omega-\omega_p}{\sigma\omega_p}\right)^2\right)}$$

where $S_{PM}(\omega)$ refers back to the PM spectrum, γ is a non-dimensional peak shape parameter, A_γ is a normalizing factor given by $A_\gamma = 1 - 0.287 \ln(\gamma)$ and σ gives the spectral width. Average data for the JONSWAP experiment data are $\gamma=3.3$, $\sigma_a=0.07$, $\sigma_b=0.09$. The different σ -values is given, depending on the angular spectral peak frequency, ω_p , and the circular frequency, ω .

$$\sigma = \sigma_a \text{ for } \omega \leq \omega_p$$

$$\sigma = \sigma_b \text{ for } \omega > \omega_p$$

The JONSWAP spectrum is expected to be a reasonable model for

Equation 19

$$3.6 < T_p / \sqrt{H_s} < 5$$

And should be used with caution outside this criterion, as the peak shape of the resulting distribution will not be realistic. (DNV, 2010)

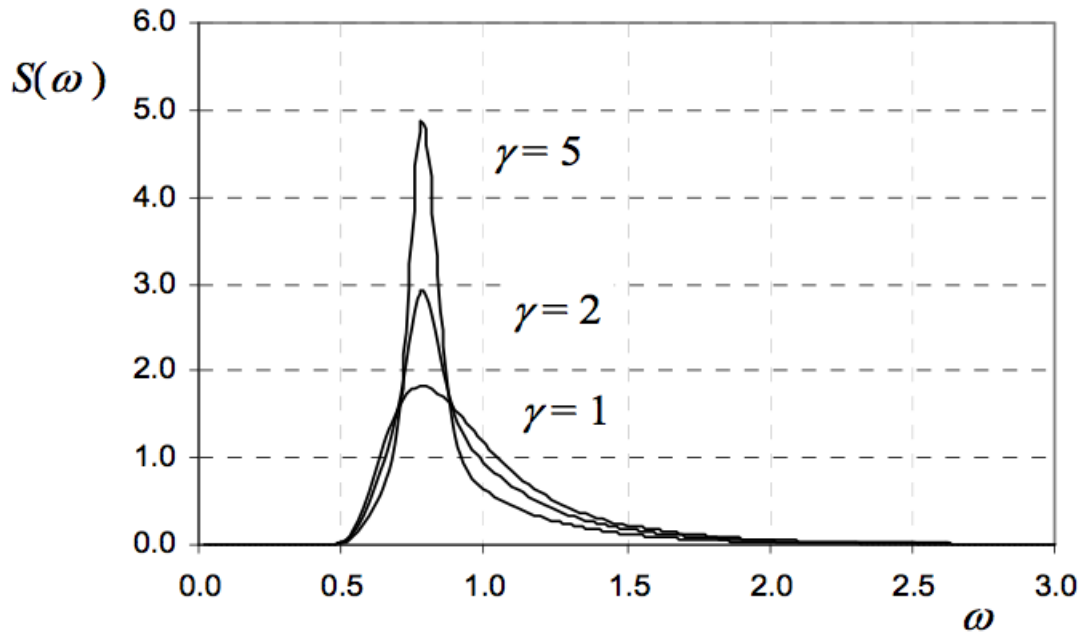


Figure 8 JONSWAP Spectrum for $H_s = 4.0$ m, $T_p = 8.0$ s for $\gamma=1$, $\gamma=2$ and $\gamma=5$. (DNV, 2010)

4.2 Wind

The wave conditions in a sea state can be divided into two classes: *wind seas* and *swell*. Wind seas are generated by local wind, while swells have no relationship to the local wind. Swells are waves that have traveled out of the areas where they are generated. (DNV, 2010)

4.3 Currents

The currents in the water column will not affect the installation phase of a pipeline project to the affect that it needs to be included in this thesis. The main factor for the installation contractor is to ensure that the pipeline stays on the proposed route, and will not drift off due to the currents.

5 Fatigue, Fracture and Material Considerations

Fracture mechanics encompass the engineering discipline of materials with cracks or flaws. Fracture mechanics allows for design and material selection while taking into account the inevitable presence of flaws. A flaw can be pores, inclusions or micro-cracks within the material. Fracture mechanics is used to calculate the stress a component with such a flaw can withstand. The key parameters for materials in regards to fracture are:

- The fracture toughness
- The stress intensity factor

5.1 Fracture Calculations

The fracture toughness is a measure related to the materials ability to withstand an applied load, while containing a flaw. While the stress intensity factor is a parameter related to the flaws ability to attract stress. This means that the flaw will act as an intensifier to the stress applied to the component. (Askeland & Phulé, 2006). The stress intensity factor can be calculated as follows

Equation 20

$$K = S\sqrt{\pi a} * F(a)$$

Where S is the stress applied, a is the crack length in the thickness direction and F(a) is a dimensionless form function related to the influence of the boundary conditions. As the fracture toughness is a material parameter and absolute, one can easily calculate the critical stress intensity.

Equation 21

$$K_c = K$$

When this condition is satisfied, the crack will start to propagate. As the fracture toughness depends on the thickness of the component, it will decrease as the thickness increases. It will decrease to a constant value called the plane strain fracture toughness, which is the usual normally reported as the property of the material. Some guidelines regarding the fracture toughness of a material is mentioned below.

- Larger flaws reduce permitted stress
- Ductile materials allows the crack tip to deform, reducing the stress intensity factor
- Impact-natured stress will reduce the fracture toughness
- Low temperature will reduce the fracture toughness

The energy related to crack growth may be regarded as the release of potential energy within the material. For an infinitesimal small amount of crack extension, the decrease in stored elastic energy of a cracked body under fixed grips conditions is equal to the decrease in potential energy under conditions of constant loading. (Berge, Fracture Design of Welded Structures, 2006) This implies that the driving force of a crack may be described as an energy release rate:

Equation 22

$$G = \left| \frac{dU}{dA} \right|$$

Crack extension will occur when G reaches the critical value G_c related to the fracture toughness. The energy release rate is directly related to the stress intensity, factor given by the Griffith/Irwin energy criterion. (Berge, Fracture Design of Welded Structures, 2006)

Fracture mechanics may be divided into two main approaches. The Linear-elastic and the Elastic-plastic fracture mechanics (LEFM & EPFM). They are divided by how they regard the size of the plastic zone at the crack tip. For the LEFM approach, plastic zone is small relative to the dimensions of the component. The EPFM approach applies to materials that exhibit time independent, non-linear behavior. This implies that the fracture will show plastic deformation prior to the actual fracture. This makes materials used in marine structures behave more in the elastic manor, rather than the linear manor.

The EPFM approach encompasses two main parameters that the LEFM do not, the crack-tip opening displacement (CTOD) and the J contour integral. For marine structures, such as pipelines, the CTOD criterion is governing. Shear forces at the tip of the crack form the crack tip opening, which in turn forms a plastic zone, blunting the crack tip. This blunting parameter is directly related to the fracture toughness of

the material. (Berge, Fracture Design of Welded Structures, 2006). The CTOD can be plotted against a non-dimensional engineering strain (e_y/e) in the component. This gives grounds for the CTOD design curve, which is the basis for the failure assessment diagram, which will be discussed later. The CTOD curve is however not a failure criterion, rather a prediction curve for the applied CTOD for a given crack length and strain. The failure criterion is given by the critical CTOD, which is determined by extensive material testing.

5.1.1 Fracture Assessment

A failure assessment diagram (FAD) governs the assessment of whether a component is likely to fracture under a given load. This diagram is based on the CTOD-curve. However, the CTOD design curve suffers from the fact that it does not include, a criterion for ductile collapse, a constant safety factor and that it is some-what outdated in regards to a two-criterion elastic-plastic failure assessment. The British Standard Institute (BSI) standard includes the CTOD curve as one of the three safety levels when it comes to fracture assessment. (British Standards Institute, 2005). These levels are:

1. FAD analysis. Intended as a screening analysis, and therefore conservative.
2. The main fracture assessment method, based on the strip-yield model.
3. Ductile tearing analysis. Highly specialized cases.

The strip-yield model is based on assuming a virtual crack, extending over the stress field of a material flaw.

5.2 Fatigue

The following theory of fatigue and its parameters is based on the work of Stig Berge.

Fatigue is a process where the material is weakened by a cyclic loading. The cyclic loading is under the ultimate tensile stress, and does not cause any short-term damage to the material. It is however, an accumulation of damage over a long period of time that will cause the structure to fail. This damage is called fatigue. Fatigue damage, along with corrosion, is the determining factor when the lifespan of a structure is calculated. This lifetime will also determine the inspection strategy for both the manufacturing and the operational stage for the component.

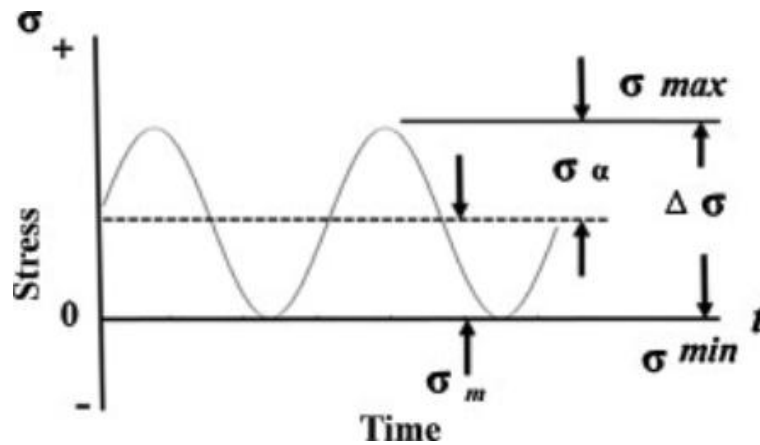


Figure 9: Cyclic Loading

5.2.1 SN-curve

A Stress-Cycle-curve or SN-curve is usually used to determine the remaining life of a component. This curve represents the finite part of the growth rate curve for a fatigue crack. This can be represented in a log-log scale.

Equation 23

$$\log(\Delta S) = -\frac{1}{m} \log N + \frac{1}{m} \log A$$

Where $\log A$ represents the intercept of the curve. This implies that the slope of the curve is $-1/m$. According to the Paris law, the remaining fatigue life of a component can be written as a sum of the number of cycles the component is subjected to, from a crack initiates to final failure.

Equation 24

$$H_g = \sum_i n_i$$

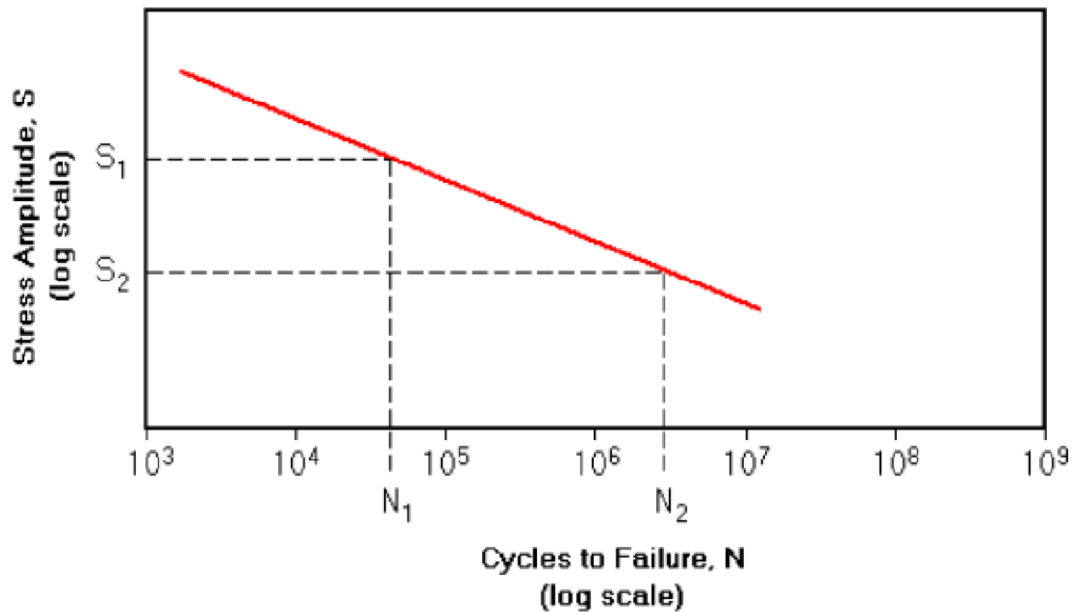


Figure 10: Example of an S-N Curve

For marine structures one often refers to the high-cycle range. This range for fatigue life is above (approximately) 10^5 cycles. Here the stress is more or less elastic, and tend to follow a log-linear curve called the SN curve.

Equation 25

$$N(\Delta S)^m = \text{Constant}$$

The low cycle range, less than 10^5 cycles, the structures will be subjected to cyclic plasticity. Here the fatigue modeling will be based on strain range, rather than the stress range of high-cycle modeling. However, low cycle fatigue can be the governing mode if the stress range of the cyclic loading is high enough.

For low stress ranges, the structure will have “infinite” life. This means that the stress will not cause enough fatigue damage over the lifetime of the structure, to cause any concern. These are often called *run-outs*, and are defined in the range of $5 \cdot 10^6$ to 10^7 cycles. This run-out range is however defined for a non-corrosive environment and may not apply for real life applications.

The fatigue damage, once accumulated enough, forms crack in the surface of the material. These crack starts along slip bands in the grains of the steel, and can result in both extruding and intruding. This is called the initiation phase of a crack.

5.2.2 The Mine Palmgren Summation

The Miner-Palmgren hypothesis uses the S-N curve of a material to predict the number of cycles it takes the material to reach failure. The term *damage* has to first be defined to perform the summation of the cycles at hand. This definition of damage is related to the damage of the *i* th cycle.

Equation 26

$$D_i = \frac{1}{N_i}$$

The Miner-Palmgren hypothesis then states that a fatigue failure is reached when the sum of the damage done by all the cycles equals one.

Equation 27

$$\sum D_i = 1$$

The S-N curve is implemented by extracting the number of cycles to failure for a specific loading from the curve. For variable loading scenarios, a number of cycles to failure is extracted for each stress range.

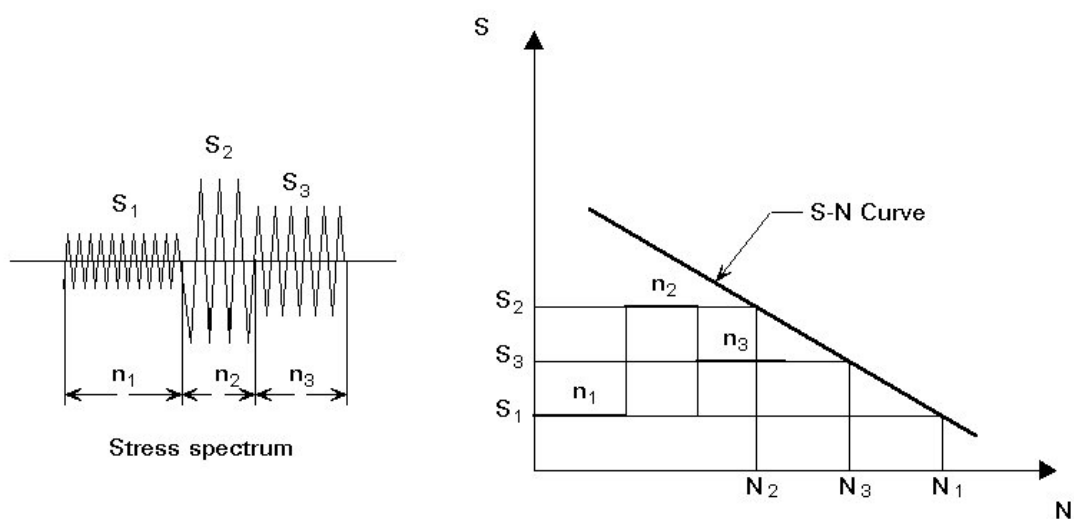


Figure 11 Miner Palmgren procedure for variable loading

5.2.3 Welded joints – Fatigue crack growth

For welded joints the initiation stage has already occurred, by the weld defects that inevitably will be present. Weld defects will always be present in some way or form. The size of these cracks can however vary from micro-crack to visible cracks. The geometry of such defects is an important parameter when it comes to the modeling of crack growth, which is normally modeled by the stress occurring at the crack tip. This relationship is given as the stress intensity factor, K.

Equation 28

$$\Delta K = \Delta S \sqrt{\pi a} F$$

Due to the cyclic nature of the loads applied, the stress intensity factor is given as a ranged value corresponding to the stress range subjected to the component. The remaining parameters in the equation are given as crack length (a) and a form function (F). The form function is dependent on external geometry, crack length and geometry, and the load configuration.

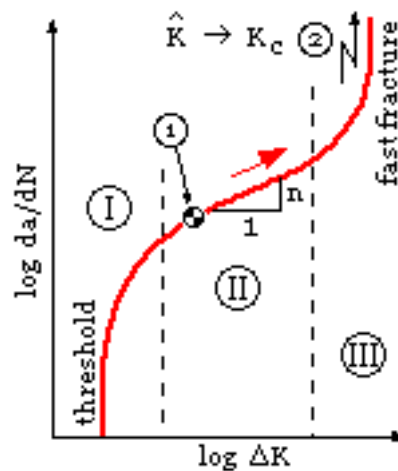


Figure 12: Crack growth rate curve (Cambridge - MIT, 2012)

The crack growth rate for a welded joint is modeled as a function of the difference in the stress intensity factor. This model can be divided into three regions, representing the different regions of the fatigue life of a joint. The regions are the threshold region, finite life region and the final failure region. In the threshold region the crack initiates, and therefore accelerates rapidly. The region is influenced by several parameters, but the main parameters are mean stress and the microstructure of the component. The

finite life region displays a constant acceleration. The crack growth relation, called the Paris-Erdogan relation.

Equation 29

$$\frac{da}{dn} = C(\Delta K)^m$$

Where C and m are material parameters. It is the Paris region is usually used for fracture assessment, i.e. the Miner-Palmgren summation. In the final failure region the crack growth rate accelerates rapidly. The governing equation is the Forman equation.

Equation 30

$$\frac{da}{dn} = C \frac{(\Delta K)^m}{(1 - R)K_c - \Delta K}$$

Where R is the stress ratio. This region shows the characteristics of an unstable fracture. This region is seldom used in practice, as failure is imminent.

5.2.4 Fatigue crack growth and inspection strategy

Fatigue design can be based on two strategies, *Safe-life* and *fail-safe*. The safe-life strategy is based on finding the typical fatigue loading the component is subjected to, and then testing the actual component in realistic conditions to estimate the actual fatigue life. The safe-life strategy also utilizes experience to add to the tests performed. This, together with a safety factor, gives a prediction of a safe-life for the component. After the estimated lifetime of the component, it is retired regardless of failure or not. A safe-life estimate is required to take the following unknown factors into account.

- Unexpected changes in load conditions
- Errors in the estimates of typical load spectra
- Scatter in test results
- Variation in properties among different batches of material
- Existence of initial defects in the production process
- Corrosion or wear
- Human errors in the operation of the component

The safe-life strategy is used on components that are difficult to inspect or repair, i.e. pipelines, risers and submerged parts of offshore structures. This is the safest strategy, but the conservatism of the safety factor also makes it the most expensive as a primary cost.

The fail-safe strategy is based on routine inspection and the possibility of repair. In addition to this, a requirement is made to ensure that if an individual member of a large structure fails, there should be sufficient structural integrity in the structure to operate safely until the crack is detected and repaired. Structures based on this strategy can be ship hulls and topside offshore structures.

5.3 NDT Testing

The welding has to be correctly executed and be inspected before the pipe length can pass through. The inspection requirement is set to 100 % by the governing standard. (DNV, 2012) The usual methods for inspection pipes are radiography (X-ray) and ultrasonic testing.

For ultrasonic testing (UT) the object is exposed to high-frequency ultrasound pulses. A transducer at the surface of the object produces these pulses. The sound waves propagate through the object, and a detector at the surface monitors their reflection patterns. Any deviation in reflection pattern indicates a defect. This test can also be automated. This requires a series of UT probes to be placed in specific areas of the weld zone. Every zone has a specific calibration reflector. A scanner is calibrated against different reference reflectors, which simulates defects. The AUT inspection is the favored inspection method by DNV. (Sævik, 2012)

The most accurate and most used test is the X-ray test. This test is performed at the last station of the firing line, just before the final tensioners. One x-ray photography take about 2-4 minutes in total from exposure to control and assessment, it is therefore allowed for some time between x-ray station to tensioner to allow for control and repair if necessary. X-ray, or radiography, requires a film to be placed under the object to be scanned. The object is subjected to radiation, which passes through the object and exposes the film. The defects in the weld will then produce a difference in exposure on the film.

Pipe diameter is a factor when it comes to X-ray testing. For small diameters (<20”) the pipe is exposed from the outside. This implies that the exposure time is longer, to allow the radiation to pass through both walls. It is also required three different exposures for each weld. This results in an extra X-ray station to be added to the firing line, in order to keep the lay rate of larger diameter pipes. For diameters above 20” if internal access is possible, one-exposure-pictures are common. (Sævik, 2012)

The NDT tests are to ensure that the workmanship is up to the requirements set by the standard. However, no NDT test will discover all defects. There is a limitation to how small the detectable defects are. These defects may cause the weld to fail by brittle, or an unstable, fracture before the theoretical maximum bending moment. Fracture mechanics based engineering criticality assessment (ECA) is needed to assess different welds with a given defect size. This will take both material curves and defect evaluations into account. The ECA evaluations and assumptions will be described in more detail later in the thesis.

5.4 Material Parameters

The general principle behind the choice of material for a pipeline is decided based on the following factors:

- Cost
- Corrosion requirements
- Weight requirements
- Weldability

Steels applied in pipelines in the offshore oil and gas industry vary from simple low-alloy carbon steels to high-alloy stainless steels, such as duplex steels. The higher alloyed steels are more expensive than the low alloy steels. This implies that the choice of the steel to be used is an important step in the design process.

The choice of steel grade will affect all phases of a pipeline project. Higher grades of steel will cost more, but may allow a reduction in the required wall thickness. The design process will define the most cost effective combination of material and fabrication cost.

During installation of the pipeline, the welding stations are a limiting factor. Higher-grade steels are more difficult to weld, and will usually return a decrease in lay-rate. From an installation aspect, lower grade steels are more preferable. But deep-water cases may require the use of higher-grade steels. This will usually also require a higher tension capacity on the lay vessel.

During the operational phase, a pipeline may be subjected to corrosion, erosion and H₂S corrosion. The pipeline may be designed to account for these effects, by adding a corrosion allowance to the wall thickness or by altering the chemical composition of the internal fluid running through the pipeline (i.e. corrosion inhibitors). (Bai & Bai, 2005)

5.4.1 Fabrication considerations

The pipeline lengths are divided into two main categories, seamless or welded. The categories are named after the method of production, where the seamless pipes do not have any welds on them. Pushing a blank piece of heated metal over a mandrel forms the inner diameter of the pipe. For the welded pipe, the blank metal ingot is either hot or cold rolled to form plates of the desired gauge. These are then bent to form a cylinder and welded along the length of the finished pipe.

5.4.2 Welding

Welding of metals and metal components is a method of joining components to each other. It can be divided into several methods, depending on the substances and materials used for the welding process. Other methods for the joining of metals exist, such as brazing and soldering, but they will not be discussed in this thesis, as they are not relevant for pipeline manufacturing.

For welding, or fusion welding, the solidification process of the metal is a key parameter. The weld is based on melting a part of the original material of the components to be joined, fusing them together. In many cases a filler material is added to the “pool” of melted metal in the joint to improve or manipulate the properties of the joint. This pool is called the fusion zone. When the fusion zone solidifies, the two original pieces of metal are joined together. During the solidification of the fusion zone, grains begin to develop. Many of the weld properties originate from the formation of these grains. The addition of chemical agents into the

weld, can manipulate the grains to grow smaller or larger in size, where smaller grains will increase the strength of the weld, but may cause some residual stress to linger in the weld. After the completion of the weld, the temperature the weld is exposed to can greatly affect the properties of the weld. A fast cooling rate results in finer grains, but will again cause some residual stress or embrittlement of the weld. While applying a post heating process to the weld, results in larger grains and higher ductility in the weld.

The method chosen for the welding, may greatly affect the properties of the finalized weld. Some methods use a low-intensity heat source, which will in turn give a longer weld time. A longer weld time will allow the heat to spread in the base metal, which will affect the grain size in parts of the base metal. The area of which the metal is affected is called the heat-affected zone (HAZ).

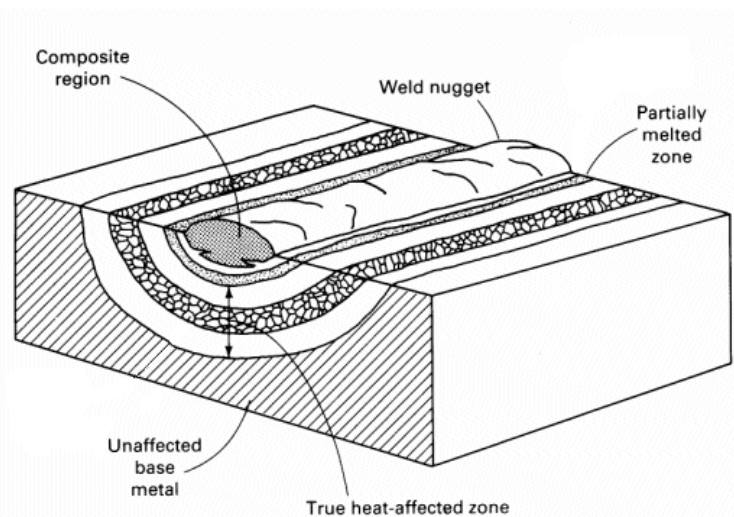


Figure 13 Heat Affected Zone and grain growth

The heat from the weld will cause grain growth in the HAZ, which will cause the properties in the zone to deteriorate. By using a more intense heat source, one can greatly decrease the amount of base metal affected by the heat. Such methods are laser and electron-beam welding. These methods however are costly and not applicable for on-site welding such as for a pipeline vessel.

The welding properties are often decided on the type of weld and the materials involved in the weld. This can be the filler materials or the base material quality. The base material property is referred to as the weldability of the metal. Many low-carbon

steels weld easily, and usually higher carbon steels are comparatively more difficult to weld. This is again due to the grains in the HAZ. Higher carbon steels will more easily form what is known as a martensitic phase in the HAZ. This phase consists of very small grains, resulting in a weldment with a poor toughness. For low-carbon steels the strength of the weld is higher than the base material. This is due to the finer pearlite microstructure that forms during cooling of the HAZ. The pearlite phase consists of ferrite and cementite, which forms lamellar grains. These grains are larger than the martensitic grains and will result in a higher toughness for the weld.

Different pre- and post- heat treatments exist to improve the properties of a weld. The methods used are case specific, and consideration of the weld method, steel alloy and weld requirements are considered. The general idea for the heat treatment is to prevent or limit the formation of the martensitic phase in the HAZ. This can be manipulated by adjusting the cooling rate of the weldment. Rapid quenching of a weld will in many cases form a martensitic phase in the weld. Applying post eating to the weld reduces the cooling rate and helps the grains in the HAZ grow to a desired size. By preheating the component, the temperature in the metal is increased prior to the welding, this will decrease the cooling rate of the weld after completion. This will also help prevent the incorporation of hydrogen in the weld. The incorporation of hydrogen into a weld causes the steel to become brittle. The high temperature of the fusion zone increases the solubility of the hydrogen atoms, allowing them to diffuse into the weld. Inside, the atoms will re-combine to form hydrogen molecules. These molecules result in a pressure increase inside the weld, causing a decrease in tensile strength and ductility. The weld will now be more likely to crack at an earlier stage than the base metal. This is known as Hydrogen Induced Cracking (HIC). In combination with external stress, it is known as Hydrogen Induced Stress Cracking (HISC).

5.4.2.1 Welding Methods

Many different welding methods exist today. The most common are Shielded Metal Arc Welding (SMAW), Gas Metal Arc Welding (GMAW), Submerged Arc Welding (SAW), Flux Cored Arc Welding (FCAW) and Gas Tungsten Arc Welding (GTAW). All of these methods are recognized by international pipeline codes and standards. (Bai & Bai, 2005)

Welding of higher grade steels require special techniques to provide satisfactory welds. These methods usually include special measures to prevent defects in the weld, such as

- Control of joint preparation and line-up
- Adequate preheating
- Additional grinding of base metal
- Careful selection of electrical characteristics
- No movement of the components until the completion of the root pass

These additional requirements may limit their usage offshore, especially when it comes to the movement of the joint prior to the root pass completion. However, the semi-automatic GMAW method is extensively used on lay barges for offshore pipeline installation. For double jointing procedures, the SAW method is used. This is a high heat and high dilution welding process, which implies that the finalized weld is dependent on the chemical composition of the base metal. Welding even higher grades of steel, such as API X80, requires careful control and check-up of the alloying elements. This is especially related to problems related to problems with the root toughness, due to the pickup of foreign elements such as aluminum.

5.4.2.2 Weld Compatibility with Corrosion Systems

Pipelines usually require a cathodic protection (CP) system to prevent excessive corrosion of the pipeline. The CP system may cause hydrogen embrittlement of the weld. This is due to the initial hardness of the weld itself, which makes it susceptible to hydrogen infusion, which in turn hardens the metal. The maximum hardness allowed for a weld varies depending on base material and operational conditions, but range from 325HV for low alloy steels to 350HV for Duplex steels. For sour-service a maximum hardness of 250HV is required due to the high corrosive nature of sour-service. Using a 10G load in a Vickers Hardness test performs all hardness tests in accordance with the standard requirements. (DNV, 2010)

5.4.3 Corrosion

Seawater is a corrosive fluid and will affect any submerged metal to a certain degree. The process is basically the degradation of the metal, where the fluid dissolves the metal until the metal is completely dissolved or the fluid is saturated with metal ions.

The corrosion will be most severe for submerged components, but corrosion will also occur on components in marine environments with air moisture, such as ships and topside offshore installations.

The corrosion process that occurs along a pipeline is known as electrochemical corrosion. In this process, an electric circuit is created between the pipe and the water surrounding it. This is now called an electrochemical cell, where the pipe wall is the anode and a fitting or a weld with a different corrosion potential than the pipe is the cathode. These two are usually connected physically, to allow electrons to flow from anode to cathode, allowing the reaction to continue. An electrolyte surrounding these components is necessary to complete the circuit. The electrolyte will allow the ions to leave the anode and form at the cathode, accepting the electrons from the anode.

The electrode potential difference between two connected metals will decide which of the two will corrode. This makes the weld design very important, as a filler metal is usually added to a weld to improve the mechanical properties of the weld. However, the addition of such a filler metal may cause the weld to differ in electrochemical potential to the base metal. This may cause the weld to become more active than the base metal, and therefore make the weld corrode faster. The weld will have a small area in relation to the base metal. In case of the weld being the anode, it will give away as many electrons as the cathode (base metal) will be able to accept. As the area of the base metal is much larger than the weld area, it will be able to accept a vast quantity of electrons. This is known as galvanic corrosion, and may cause severe corrosion rates at very localized areas. This principle may also be utilized as a design measure to prevent excessive corrosion rates. This is done by making the weld the cathode and the base metal the anode. As the corrosion rate is given by how many electrons the cathode is able to accept from the anode, the small area of the cathode will limit the amount of electron given away by the anode, reducing the corrosion rate.

In some cases, intergranular corrosion may occur. This is a highly localized corrosion mode, which will occur at the boundaries between the grains of the metal. This corrosion mode may act as the start or initial state of a crack, and may cause some high corrosion rates. The reason for the high corrosion rates is that the crack may have a lower oxygen concentration than the surroundings. This phenomenon is called

crevice corrosion may cause accelerated corrosion at the crack tip. (Askeland & Phulé, 2006)

5.4.3.1 Corrosion Protection

A series of different measures may be taken to prevent corrosion, such as coatings, inhibitors and cathodic protection. But the most important and basic protection is the material selection. This selection should prevent the formation of galvanic cells, i.e. using similar metals or alloys. Another basic rule of thumb is to make the anode area much larger than the cathode area, as this will limit the amount of corrosion of the weld.

Coating of a component will limit the corrosion by isolating the metal from the corrosive fluid. However, a scratch or discontinuity in the coating will allow for a small anodic site to be exposed and will undergo a rapid and very localized corrosion.

Internal corrosion of a pipeline may be limited by adding an inhibitor to the internal fluid. The inhibitor is chemically built to either migrate to the cathode or anode, covering the part and insulating it from the original fluid. This will act the same way as a coating but requires a certain concentration of inhibitor, and will not be permanent.

A commonly used protection system for pipelines is cathodic protection. This is usually done by using a sacrificial anode attached to the base metal, allowing the anode to corrode. The corrosion of the anode will supply the base metal with electrons, forcing the base metal to become the cathode and therefore limiting the corrosion of the pipeline. The sacrificial anode, usually zinc or magnesium, is depleted over time and must eventually be replaced. (Askeland & Phulé, 2006)

5.5 Engineering Criticality Assessment (ECA)

The ECA method was developed to assess whether a weld with a certain flaw size could withstand the extreme- and operational loads of a design scenario. The maximum flaw size that can take these loads defines the acceptance criteria of the weld. This criterion then defines the calibration base for the different NDT tests. For installation assessment, the procedure will provide information on the flaw size to be expected in the pipeline after installation. This is essential for the assessment of the operational phase of the pipeline. The recommendation is that the flaw size shall be

less than 1 mm for the installation phase. (DNV, 2006) The whole ECA process is to be assessed by a sensitivity analysis after completion, to ensure that small deviations in assumptions will not have significant influence on the analysis and conclusions made. (Reinertsen, 2010)

The final assessment of the flaw size is made by a failure assessment diagram (FAD). This diagram considers both the stress-strain diagram and the CTOD-R curve. The CTOD-R curve is a function of the displacement at the crack tip opening. The FAD diagram can be used at different levels, considering different safety levels for the flaw size. The recommended level for installation assessment is level 3B. (Berge, Fatigue Design of Welded Structures, 2006) (British Standards Institute, 2005) This level considers a tearing analysis based on a reference material of FAD. It is common to assume the same strength properties as for the parent pipe material when analyzing the weld. (DNV, 2006) This is based on that the strength of the material varies over the HAZ. Since the location of the flaw is hard to determine exactly, the use of the FAD will give a conservative result.

When considering cyclic loading, the stress-strain curve for the material will change due to the Bauschinger effect. This effect normally decreases the yield strength of a material about 15-20%. The tensile strength is however unaffected. The Bauschinger effect is also described under section 6.1.3 below. This effect needs to be considered when assessing the weld. It is however normal to use the stress-strain curve for the “as received” pipe material. (DNV, 2006)

6 Nonlinear finite element method

The content in this chapter will cover a few fundamental aspects of the finite element method. It will not cover the subject in depth as it is assumed that the reader has a certain understanding of the subject.

6.1 Basics of the Finite Element Method

The finite element method is based on three fundamental concepts.

- Equilibrium considerations
- Kinematic compatibility
- Constitutive Equations

6.1.1 Equilibrium

The equilibrium considerations are the same as for the basic mechanics. In the finite element method it is expressed by the principle of virtual displacements. This principle states that the work performed by the constant true internal stress and constant external force is zero when the structure is exposed to a virtual displacement field, which also satisfies the boundary conditions. The principle is valid when the internal and external forces represent an equilibrium state. In SIMLA, the volume forces are neglected, while the initial stresses are considered.

6.1.2 Kinematic compatibility

The compatibility concept ensures that the adjacent cross-sections of a beam are deformed equally, and that the material is continuous during deformation. Applying interpolation functions and finite strain along the boundaries of the element ensures the displacement continuity. SIMLA employs the Bernoulli-Euler deformation hypothesis, in its analysis. This hypothesis assumes that plane cross-sections perpendicular to the neutral axis, remain plane and perpendicular to the neutral axis after deformation. This will neglect the shear deformation. SIMLA will also apply the Green strain definition to neglect the 2nd order longitudinal engineering strain.

Equation 31

$$E_{xx} = u_x - yv_{xx} - zw_{xx} + \frac{1}{2}(v_x^2 + w_x^2) + \theta_x(yw_x - zv_x) + \frac{1}{2}\theta_x^2(y^2 + z^2)$$

This equation is based on the Bernoulli-Euler requirement, which also applies in the elastoplastic area. Here, the neutral axis coincides with the x-axis, while u, v and w are the axial, horizontal and vertical displacements and the θ represents the torsional rotation around the neutral axis.

6.1.3 Constitutive Equations

The stresses in the equilibrium considerations have to be related to the strain within the structure. For an elastic case, the relation can be handled by introducing Hooke's law. For a pipeline, the effect of internal and external pressure will result in a circumferential stress resultant. For an elastoplastic case the circumferential stress resultant must be included in the formulation of the model. For nonlinear problems, incremental methods are used. Such methods require the plastic strain to be calculated for the entire load history. The definition of three features is needed to calculate the plastic strain history.

- An initial yield criterion
- A hardening rule
- A flow rule

The initial yield criterion defines the stress state where the plastic deformation first occurs. The stress tensor in a steel structure can be expressed by both the 2nd Piola-Kirchoff and the Cauchy stress tensor, as the strain in such a structure is usually so small that the two tensors coincide. The 2-dimensional von Mises yield criterion is then expressed as

Equation 32

$$F_{initial} = \sqrt{\sigma_1^2 + \sigma_2^2 - \sigma_1\sigma_2} - \sigma_Y = 0$$

As the plastic flow proceeds, the material may experience hardening. This will alter the yield criterion as the loading occurs. This can be modeled by either an isotropic or kinematic hardening model, both included in SIMLA. The following figure illustrates

the two concepts for a uniaxial state of stress.

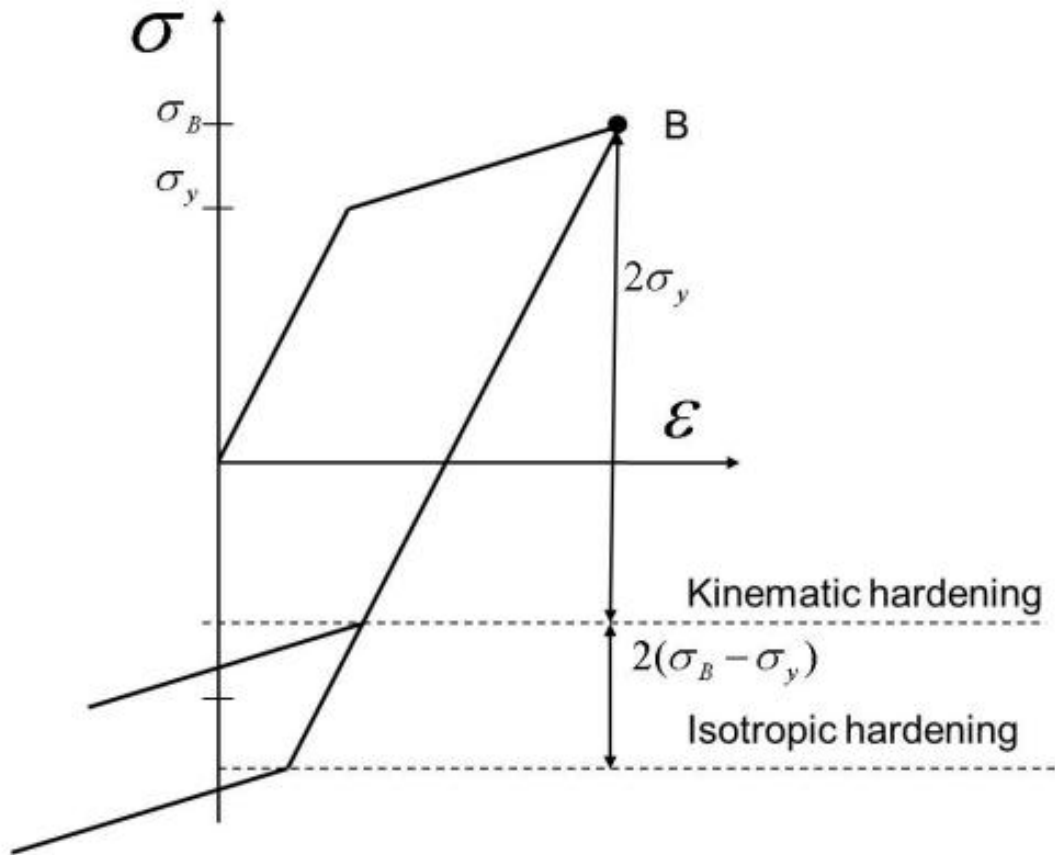


Figure 14: Kinematic and isotropic hardening a uni-axial case (Sævik, 2012)

The main difference in the two models is evident when the loading is reversed. For an isotropic model the yield criterion will be unaltered, while for a kinematic model the criterion will be decreased during the reversal of the loading. The elastic range of the stress state will then be equal to two times the original yield strength of the material. This effect is often referred to as the previously mentioned, *Bauschinger effect*.

The flow rule of the plastic strain determines the increment to be used for the load history. The starting point of the flow rule is to define the yield surface. SIMLA assumes the yield surface to depend on the 2nd deviatoric stress invariant J_2 , and a hardening parameter κ .

Equation 33

$$f(J_2, \kappa) = 0$$

The domain of this function is given as follows:

- $f < 0$: Elastic range
- $f = 0$: Plastic range
- $f > 0$: inadmissible

Further the function is dependent on Drucker's postulate of a stable material, which assumes:

- The yield surface is convex
- The plastic strain increment is normal to the yield surface
- The plastic strain increment is a linear function of the stress increment

The above-mentioned derivation of the flow rule is thoroughly described in the SIMLA theory manual and will not be further discussed in this thesis (Sævik, 2012). The result of the derivation and the constitutive equation describing the relation between the total strain increment and the stress increment is given below on component form.

Equation 34

$$\Delta\sigma_{ij} = D_{ijkl}(E_{ijkl}, \sigma, \kappa)\Delta\epsilon_{kl}$$

For the elastic range, the incremental equation is given by Hooke's law.

6.2 Total Lagrangian (TL) and the Updated Lagrangian (UL) formulations

The two methods used for the nonlinear finite element problem differ in the choice of reference configuration. The TL formulation refers a new configuration back to the original configuration (C_0). The UL formulation refers to the previous configuration that satisfied equilibrium (C_n). Several variations and approaches to these formulations exist to improve efficiency of the computer codes, but the principle remains the same, to separate rigid body motions from the local or relative deformation of the element. By fixing a local coordinate system to the element and letting it deform and rotate with the element as the element deforms, one can separate the nonlinearities arising from large displacements from the nonlinearities within the element. This gives grounds for several terms describing the method, such as the Co-rotational Formulation and the Co-rotated Ghost Reference Formulation (Mathisen, 1990).

SIMLA bases its calculations on a co-rotational reference model. This approach resembles the UL formulation as it uses a fixed coordinate system and continuously updated as the deformation occurs. For small strain values the difference in the two formulations is negligible. The coordinate system in the co-rotational formulation is defined such that the longitudinal axis intersects the end nodes of the element at the last known equilibrium configuration. This definition of the coordinate system separates the rigid body motions from the relative deformation of the element.

6.3 Dynamic Analysis

Both static and dynamic analyses should always be performed in pipeline design. The dynamic analysis requires a mass matrix to be established. This can be done by either considerations regarding the kinetic energy in the system or by utilizing the Principle of Virtual Displacement. The establishment of the mass matrix is given, on element level, as

Equation 35

$$m = \int_{V_0} \rho_s N^T N dV \quad u = Nv$$

The ρ is the structural density and N is the interpolation function matrix. This matrix relates the nodal degrees of freedom to the displacement vector at arbitrary locations within the element. For underwater problems a hydrodynamic mass matrix is needed as well.

SIMLA uses Rayleigh's proportional damping and concentrated damping to formulate the structural damping of a system. For a linear problem, Rayleigh damping can be used, as this will yield an uncoupled system of equations can be found if the eigenmodes of the system are known. The uncoupled equation responses may then be superposed to give the total solution.

A non-linear dynamic model cannot be solved by the previous mentioned approach, as the principle of modal superposition is not valid. This implies that the low frequency modes are damped out by proportional mass damping. Also the higher frequency modes are damped out by a proportional stiffness damping. This stiffness damping is usually introduced as a Rayleigh damping, corresponding to the following equation.

Equation 36

$$C = C_0 + \zeta_1 M + \zeta_2 K_T$$

The global equilibrium is given by the dynamic equilibrium equation. Here, all the element contributions are added into the matrix system, and expressed as

Equation 37

$$M\ddot{r} + C\dot{r} + R^I = R^E$$

Here M is the global mass matrix, C the global damping matrix, R^I a vector describing the internal forces and R^E a vector describing the external forces. For a nonlinear dynamic analysis, this equation is solved by an incremental progression over time. The internal forces are found by the summation of these increments used to calculate the given equilibrium state.

6.4 Solution Methods

As a dynamic problem cannot be solved by modal superposition, a direct time integration of the equation of motion is necessary. This can be done by either using an explicit method or by implicit methods.

The explicit method determines the displacement at the next time increment by utilizing the information at the current and previous time steps. The explicit method is conditionally stable and will therefore require small time increments. Formulating these methods using lumped mass and damping matrices, one can limit the computational time required. This is due to the fact that the coupled equation system in the time steps does not need to be solved, hence very little computational effort is required. The typical use for an explicit method is for explosion or impact analysis.

The implicit method calculates the displacements by using information given for the next time step, in addition to the information given on the current time step. This results in a better numerical stability than explicit methods. Several versions of the implicit exist. They differ in the way they assume acceleration variations between the time steps and at which time the equilibrium equation is satisfied. This can be utilized by assuming constant average acceleration, which makes for an unconditionally stable result. This is especially beneficial for long analysis durations. However, for implicit

methods, the coupled equation system is required to be solved at every time step. This makes the method economically undesirable for short time analysis. (Sævik, 2012)

For a nonlinear dynamic analysis, the higher mode results are often not as important as the lower mode results. To limit the computational effort required, it is often desirable to remove the higher order frequencies. A numerical damping scheme will remove the higher order modes, but also reduce the accuracy of the lower modes. In order to preserve the accuracy a method referred to as the HHT- α method is introduced. In SIMLA this method is used in a time integration scheme. As the system equilibrium equation is nonlinear, the solution is obtained by an incremental method. This whole scheme is described in the PhD dissertation of Kjell Magne Mathisen, and will not be discussed further in this thesis.

6.5 Pipe Element

When modeling the bending of a pipeline the Bernoulli-Euler assumption where plane planes remain plane and perpendicular to the neutral axis, apply. This also implies that shear deformations can be neglected and shear forces must be calculated by equilibrium considerations of the element-bending gradient. This, in addition to Navier's hypothesis, can describe the motion of an arbitrary point in the pipe cross-section by the displacement quantities for the centerline of the element. This, in addition to the Green strain tensor and expressions for the 2nd Piola-Kirchoff stress, the incremental equation for non-linear solutions and the material law, gives the background for the interpolation functions that describes the deformations of the element. The longitudinal interpolation function is normally linear, while the transverse function is described by a cubic function. This implies that the axial strain is constant and the curvature is linear. For plastic behavior, the material model needs to include memory effects and the stiffness and equilibrium forces need to be evaluated by numerical integration.

6.6 Nonlinearities

As mentioned above the pipeline analysis done in this thesis will be based on a nonlinear model, as the long and slender nature of subsea pipelines makes them susceptible to nonlinear effects. Such effects are:

- Non-linear pipe-soil interaction
- Non-linear hydrodynamic loading
- Varying boundary conditions
- Different pressure and temperature forces due to variation in fluid flow

Considering the nature of the S-lay installation process, the large displacement non-linearity is easy to imagine. This causes issues when relating the local stresses to the global axis. As the pipeline leaves the vessel it enters a slope, which causes the local axis of an element differ from the original axis. This implies that a term needs to be introduced to describe the transformation into the sloped configuration, to continue to describe the equilibrium. The term is a stress measure related to the rigid body motion of the pipe entering the slope and refers back to its reference position. In short, the stress components in the sloped configuration still have to refer to the same stress components as for the original configuration.

The stress and strain in the pipeline in the S-lay configuration may enter the plastic zone of the steel. Here the material will behave in an elastic-plastic manor. In addition to this, the hoop stress and the longitudinal stress cause the pipeline to be subjected to a two-dimensional state of stress. Hence, a two dimensional, elastic-plastic material model has to be used.

The hydrodynamic loading of the pipeline that already has entered the sea is also a source of non-linearities. These include drag-forces and wave induced current velocities. The drag is proportional to the relative velocity between the water and the pipe, while the wave induced current velocities also will include higher order Fourier components.

Several software codes have been developed to consistently take all these non-linear aspects into account. In addition to the SIMLA code, ABAQUS and ANSYS are some examples of the more multipurpose programs capable of handling advanced non-linear pipeline design. However, SIMLA also enables route planning and design analysis throughout all phases of installation and operation. (Sævik, Økland, Baarholm, & Gjøsteen, 2012)

7 LINKpipe

Traditionally, the rules of defect assessment allowed for no defect present in a load-condition causing inelasticity. Therefore, advanced numerical assessments are needed to assess certain problems. Finite element models are traditionally used. Here, the shell structure is discretized by three-dimensional solid elements in order to account for the crack. The figure below shows a typical mesh configuration.

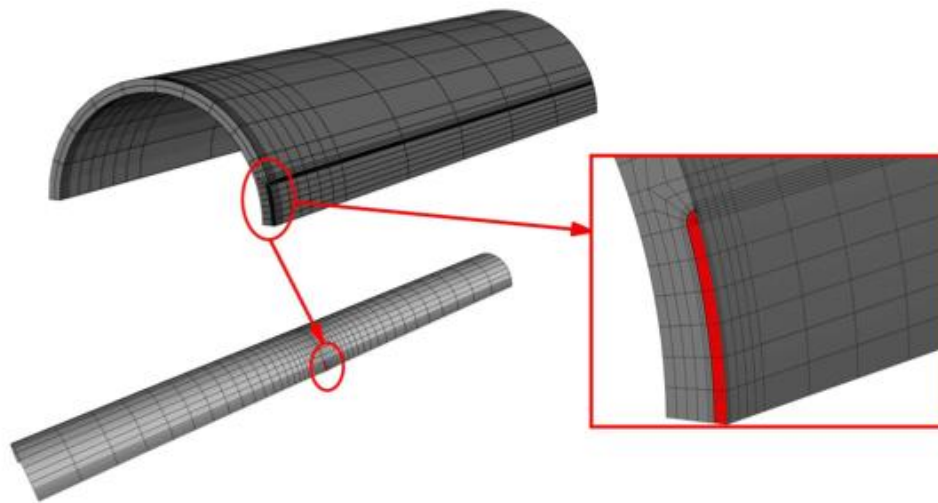


Figure 15 Typical mesh in LINKpipe

The solid nature of the elements in such a model, may cause complicated pre- and post-processing of the model, in addition to a long CPU time. To compensate for this, shell elements may be utilized. This will however complicate the representation of the crack itself. To make the model as effective and accurate as possible, line-spring elements is used at the crack location. Whereas a solid element model may have 30000 degrees of freedom, the shell and line-spring model may have only 1000. This is due to the choice of elements and the utilization of symmetry in the model. Therefore the CPU time may be reduced and the pre- and post-processing is left much less complicated.

The three-dimensional problem is simplified by formulating it as a two-dimensional plate or shell theory problem, where the crack is represented by line-springs elements at the crack location. The line-spring element can be regarded as two straight lines

connected to each other by a series of springs.

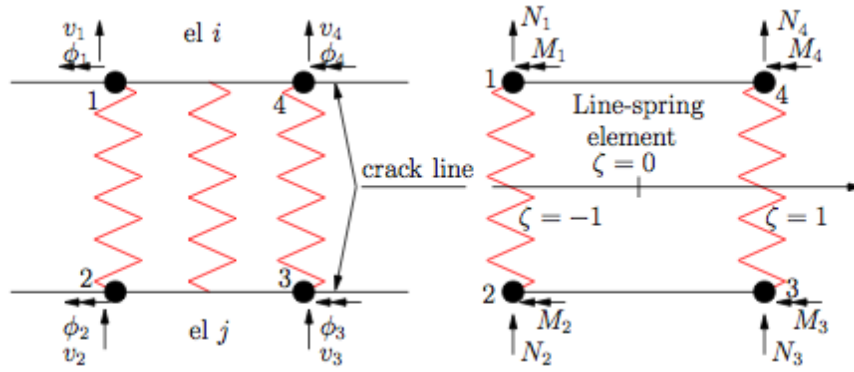


Figure 16 Line-spring elements

When a crack starts to open, the lines move apart. The springs will constrain this displacement, representing the materials crack toughness. The 4-node shell element represented above has corresponding 4-noded line-springs, with linear interpolation polynomials. To give an accurate representation of the actual problem, a 2-point Gaussian integration is employed. The line-spring element now has 8 degrees of freedom, with four in-plane displacements and four rotational around the longitudinal axis.

7.1 Generalized displacements and interpolation functions

The numerical interpolation between the nodal displacements or forces and the generalized is done by a Gauss quadrature, and linear interpolation is used when the integration points are located at the following positions.

Equation 38

$$\zeta_A = -\frac{1}{\sqrt{3}}, \quad \zeta_B = \frac{1}{\sqrt{3}}$$

then the generalized displacements in the line-spring element can be expressed as

Equation 39

$$q_A = \begin{bmatrix} \delta_A \\ \theta_A \end{bmatrix}, \quad q_B = \begin{bmatrix} \delta_B \\ \theta_B \end{bmatrix}$$

The relationship between the nodal displacements (v_i, ϕ_i) and the generalized displacements are expressed as

Equation 40

$$\delta^* = N^* v_e$$

where the components represents matrices as follows

Equation 41

$$\delta^* = \begin{bmatrix} \delta_A \\ \theta_A \\ \delta_B \\ \theta_B \end{bmatrix} \quad N^* = \begin{bmatrix} 1 & 0 & -1 & 0 & 0 & 0 & 0 & 0 \\ 0 & 1 & 0 & -1 & 0 & 0 & 0 & 0 \\ 0 & 0 & 0 & 0 & -1 & 0 & 1 & 0 \\ 0 & 0 & 0 & 0 & 0 & -1 & 0 & 1 \end{bmatrix} \quad v_e = \begin{bmatrix} v_1 \\ \phi_1 \\ v_2 \\ \phi_2 \\ v_3 \\ \phi_3 \\ v_4 \\ \phi_4 \end{bmatrix}$$

The generalized displacements at an arbitrary point is expressed as

Equation 42

$$q = N \delta^*$$

where

Equation 43

$$q = \begin{bmatrix} \delta(\zeta) \\ \theta(\zeta) \end{bmatrix} \quad N = \begin{bmatrix} \hat{N}_1 & 0 & \hat{N}_2 & 0 \\ 0 & \hat{N}_1 & 0 & \hat{N}_2 \end{bmatrix} \quad \delta^* = \begin{bmatrix} \delta_A \\ \theta_A \\ \delta_B \\ \theta_B \end{bmatrix}$$

The quantities \hat{N}_1 and \hat{N}_2 are expressed as (Rice, 1972)

Equation 44

$$\hat{N}_1 = \frac{1 - \zeta}{2} \quad \hat{N}_2 = \frac{1 + \zeta}{2}$$

and represent the interpolation polynomials of the element in question.

7.2 Generalized forces

The internal forces within the line-spring element is derived from the generalized displacements, and therefore regarded as generalized forces. The forces are computed from the displacements, \mathbf{q} at a arbitrary point $|\zeta| \leq 1$ as

Equation 45

$$\mathbf{Q} = \mathbf{D}\mathbf{q}$$

where \mathbf{D} equals the stiffness matrix of the line-spring element. Combining this equation with the previous expressions for the relationship between nodal displacements and the generalized displacement, and the generalized displacements at an arbitrary point, yields a relation for the generalized forces in the line-spring element as follows

Equation 46

$$Q = DNN^*v_c$$

Where the matrix multiplication NN^* equals $N^{**} = ([N], -[N])$.

The nodal forces in the line-spring element are derived from the generalized forces. Where the general expression can be expressed as

Equation 47

$$\begin{bmatrix} N_1 \\ M_1 \\ N_4 \\ M_4 \end{bmatrix} = - \begin{bmatrix} N_2 \\ M_2 \\ N_3 \\ M_3 \end{bmatrix} = \int_{LS} \begin{bmatrix} \hat{N}_1 & 0 \\ 0 & \hat{N}_1 \\ \hat{N}_2 & 0 \\ 0 & \hat{N}_2 \end{bmatrix} \begin{bmatrix} N \\ M \end{bmatrix} ds$$

where $[N, M]^T$ are the generalized forces, \mathbf{Q} . The total nodal force vector from the line-spring element is then expressed as $\mathbf{F}_e = [N_1, M_1, N_2, M_2, N_3, M_3, N_4, M_4]^T$.

where the matrix multiplication expression reads

Equation 48

$$F_e = \int_{LS} \begin{bmatrix} [N^T] \\ -[N^T] \end{bmatrix} \begin{bmatrix} N \\ M \end{bmatrix} ds$$

This will, by combining the equation above with the expression for the generalized forces in the line-spring element, give the nodal force equation

Equation 49

$$F_e = \int_{LS} N^{**T} D N^{**} ds v_e$$

7.3 The linear elastic line-spring

When the component is exposed to loading causing strain in the elastic domain, the work will be described using a compliance matrix, C

Equation 50

$$C = \begin{bmatrix} C_{NN} & C_{NM} \\ C_{MN} & C_{MM} \end{bmatrix}$$

C is a symmetric matrix where the terms for C_{ij} are determined from the stress intensity calibrations of SEN specimen test. These tests use the energy/compliance relationship proposed by Rice (Rice, 1972).

This compliance matrix gives the grounds for the connection of displacements and forces in the element, using the following formula

Equation 51

$$q = CQ$$

For the load controlled situation the energy release rate is described as follows

Equation 52

$$\zeta = \frac{1}{2} Q \frac{\partial q}{\partial a}$$

Where Q and q are given as

Equation 53

$$Q = [N, M]^T$$

$$q = [\delta, \theta]^T$$

The generalized forces and displacements can now be written, using the compliance matrix, as follows

Equation 54

$$\delta = C_{NN}N + C_{NM}M$$

$$\theta = C_{MN}N + C_{MM}M$$

$$C_{NM} = C_{MN}$$

Using these previously described formulas; the complete expression for the energy release rate can now be written as

Equation 55

$$\zeta = \frac{1}{2} \left(N^2 \frac{\partial C_{NN}}{\partial a} + 2NM \frac{\partial C_{MN}}{\partial a} + M^2 \frac{\partial C_{MM}}{\partial a} \right)$$

From fracture mechanics, the connection between ζ and stress intensity factor can be used to derive the elastic compliances as follows

Equation 56

$$K_{I,N} = \frac{N}{t} \sqrt{\pi a} f_N = \sigma_N \sqrt{\pi a} f_N$$

$$K_{I,N} = \frac{M}{\frac{1}{6}t} \sqrt{\pi a} f_M = \sigma_M \sqrt{\pi a} f_M$$

Here, the functions f_N and f_M are polynomials of crack depth to thickness ratio. These functions are found in handbooks such as Tada et al (H. Tada, 1985). (B. Gross, 1965) The most common and the ones used in LINKpipe are

Equation 57

$$f_N = 1.122 - 0.231 \left(\frac{a}{t}\right) + 10.550 \left(\frac{a}{t}\right)^2 - 21.710 \left(\frac{a}{t}\right)^3 + 30.382 \left(\frac{a}{t}\right)^4$$

$$f_M = 1.122 - 1.40 \left(\frac{a}{t}\right) + 7.33 \left(\frac{a}{t}\right)^2 - 13.08 \left(\frac{a}{t}\right)^3 + 14.0 \left(\frac{a}{t}\right)^4$$

The energy release rate can now be expressed by using the stress intensity factor

Equation 58

$$\zeta = \frac{K_I^2}{E'} = \frac{\pi a}{E'} (\sigma_N^2 f_N^2 + 2\sigma_N \sigma_M f_N f_M + \sigma_M^2 f_M^2)$$

There now exist two expressions for the energy release rate. These two can be combined to give the expressions for the components in the compliance matrix.

Equation 59

$$C_{NN} = \frac{2\pi}{E't^2} \int_0^a a f_N^2 da$$

$$C_{MN} = \frac{2\pi}{E' \frac{1}{6} t^3} \int_0^a a f_N f_M da$$

$$C_{MM} = \frac{2\pi}{E' \frac{1}{36} t^4} \int_0^a a f_M^2 da$$

The stress intensity factor for a single edge crack, may now be described by

Equation 60

$$K_I = \sqrt{t} \left(\frac{N}{t} k_N + \frac{6M}{t^2} k_M \right)$$

where the two k parameters are functions describing the crack depth to the thickness of the specimen. They have been thoroughly described by Gross and Srawley (B. Gross, 1965), but may also be obtained from handbooks such as Tada et. al (H. Tada, 1985). The general equations describing these parameters are

Equation 61

$$k_N = \sqrt{\frac{a}{t}} \left(1.99 - 0.41 \left(\frac{a}{t} \right) + 18.70 \left(\frac{a}{t} \right)^2 - 38.48 \left(\frac{a}{t} \right)^3 + 53.85 \left(\frac{a}{t} \right)^4 \right)$$

$$k_M = \sqrt{\frac{a}{t}} \left(1.99 - 2.47 \left(\frac{a}{t} \right) + 12.97 \left(\frac{a}{t} \right)^2 - 23.17 \left(\frac{a}{t} \right)^3 + 24.80 \left(\frac{a}{t} \right)^4 \right)$$

The crack will behave as if it is deeper than it actually is, due to the local plasticity ahead of the crack tip. This will occur even at elastic loads levels. This phenomenon requires an assessment of how deep the crack actually affects the material. A modified crack depth formulation for the line-spring element is introduced into the calculations by

Equation 62

$$a_{eff} = a_0 + 0.0195 \left(\frac{K_I(a_{eff})}{\sigma_0} \right)^2$$

This is usually referred to as an Irwin correction. A Newton-Raphson iteration scheme is used to compute a_{eff} , which is then used in the following computations of the line-spring element.

In the case of a plane strain scenario, the J-integral is connected to the stress intensity factor through

Equation 63

$$J_{el} = (1 - \nu^2) \frac{K_I^2}{E}$$

the same principles used in the derivation of the stress intensity factor can be applied for the T-stress evaluation of surface cracked plates and shell structures. The T-stress is the first non-singular term in the William's eigenvalue expansion of the crack tip stress field. Thus, the T-stress is the summation of the generalized force contributions, resulting in the following expression of the T-stress at any given point along the crack front

Equation 64

$$T = \frac{N}{t} t_N + \frac{6M}{t^2} t_M$$

where the t_N and t_M are calibration factors for the T-stress in a single-edge-notch specimen test, with the same thickness to crack depth ratio and membrane stress, bending loads. Some of these values are tabulated by Sham (Sham, 1991), giving grounds for the polynomial derived by (Y. Wang, 1992).

Equation 65

$$t_N = -0.501 - 1.842 \left(\frac{a}{t} \right) + 14.48 \left(\frac{a}{t} \right)^2 - 45.03 \left(\frac{a}{t} \right)^3 + 47.42 \left(\frac{a}{t} \right)^4$$
$$t_M = -0.505 - 0.906 \left(\frac{a}{t} \right) + 3.637 \left(\frac{a}{t} \right)^2 - 10.73 \left(\frac{a}{t} \right)^3 + 14.08 \left(\frac{a}{t} \right)^4$$

These polynomials were derived for the crack depth to thickness ratio of 0.1 to 0.8. A significant deviation between the line-spring model and the 3D continuum models for crack depth to thickness ratios above 0.6 was shown and implemented in the LINKpipe code.

7.4 Solution Techniques

The global response curve for the simulation of the crack includes limit points, such as global or local instabilities. In order to ensure that these points do not result in divergent solutions, the Newton-Raphson iterations have to be modified. This can be done by the Riks arc length method or by the improved Fieds method. The iteration process is modified to better estimate the new equilibrium, using the tangential value for the last equilibrium step. During the iterations the external load level and the incremental solution vector are adjusted, making sure the displacements and rotations are in equilibrium with the load level.

For a nonlinear problem, the structural response may change greatly from the linear elastic range to the nonlinear range. The size of the load increment is therefore an important parameter, and needs to be kept small enough to capture the behavior of the model accurately. In addition to the size of the increment step, the governing degree of freedom needs to be selected with care. This degree of freedom may be selected based on the expected response and the direction of the nonlinear response.

8 SIMLA Model

8.1 Model Background

The calculation model to be used will be based on realistic cases taken from the Ormen Lange oil field, 120 km west of Mid-Norway. This field features a subsea tie-back to the onshore terminal at Nyhamna, as well as a field extension which connects the original tie-back pipeline to the new production systems located south of the tie-back. The extension includes a 16” production flowline, installed in 2009, which will be subject to the calculations done in this thesis.

For the installation phase of the project (laying only), a maximum allowance of 10 % consumption of total fatigue life was set. (DNV, 2010) During installation the pipeline was empty, and flooding of the pipeline was done after lay-down.

The design life of all pipelines, spools and umbilical’s in the Ormen Lange Southern Field development was set to 30 years. The material data for the proposed pipelines material is given in the table below.

Table 2 Pipe material data

Parameter	Unit	Flowlines
DNV Material grade	N/A	SML 450 IDF
Fabrication method	-	Seamless
Steel Density	kg/m ³	7850
Young’s Modulus	GPa	207
Thermal Expansion (20 ^o)	°C	11.7*10 ⁶
Thermal Conductivity	W/mK	45-50
SMYS	MPa	450
SMTS	MPa	535
Poisson’s ratio	-	0.3
Material strength factor, α	-	0.96

The stress strain relationship for the pipeline design is assumed and based on a piece-wise curvefit, defining the relationship as:

Yield stress = 0.2% strain

Tensile stress = 10% strain

The pipeline dimensions and characteristic data are given in the table below.

Table 3 Pipe characteristics

Characteristics	Pipelines
Nominal size	16 inch
Internal diameter	355.6 mm
DNV Material Grade	SML, 450 IDF
Wall thickness	23.0 mm
Fabrication tolerance	10%
Out-of-roundness from fabrication	2.4 mm
Protection and corrosion coating	0.3 mm FBE / 7.7 mm PP

This thesis will not take the pipeline coating into account, as it will not contribute to the fatigue life of the pipeline. This also applies for the insulation of the pipeline.

The pipeline is protected by a cathodic protection system, in accordance with NORSOK M-503, between 850 mV and -1100 mV.

Table 4 Tension parameters

Parameter	
Depth [m]	880
Wall Thickness [mm]	23
Submerged Weight [N/m]	851
Bottom Tension [t]	8.9
Top Tension [t]	85.2
Catenary Length [m]	977
Top Angle [°] ³	84
Layback Length [m]	129

8.2 Wave data

The waves used in this thesis will be based on the JONSWAP spectrum. Two significant wave height values will be assessed, with varying wave period.

Table 5 Analysis matrix

Analysis	1	2	3	4	5	6	7	8	9	10
H _S [m]	1.5	1.5	1.5	1.5	1.5	2.5	2.5	2.5	2.5	2.5
T _P [s]	5	8	9	10	13	5	8	9	10	13

The T_P values are chosen to reflect a range of probable response values, based on the vessel RAO and the two JONSWAP distributions. The wave data presented in this section is valid for most of the pipeline route, except from the near-shore sections.

³ The angle given in the table above is the angle from the surface to the stinger tip

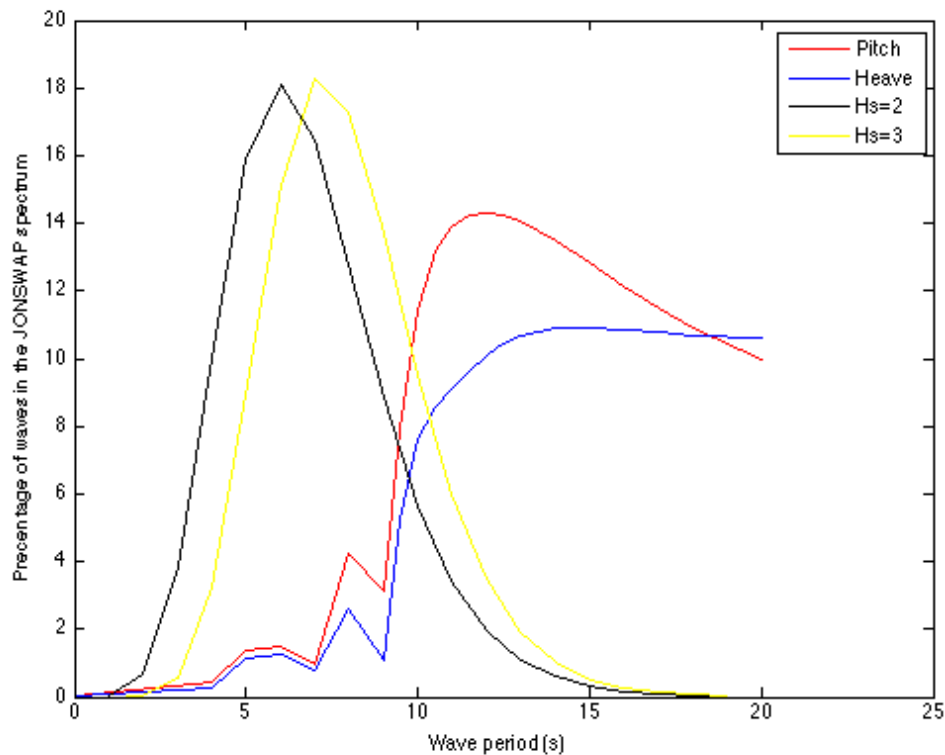


Figure 17 JONSWAP spectrum and pitch and heave RAOs. The RAOs remain dimensionless for the presentation purpose

The seabed will remain plane in the analyses presented in this thesis. This is to ensure that the results are comparable and that the trend they will provide will be more obvious. The seabed topography may increase or decrease the load on the pipeline catenary, as the pipeline may display a different behavior when it is run over undulated areas such as free spans.

8.3 SIMLA model

The model used for this thesis is based on a model used by MARINTEK to compare SIMLA to another code, OFFPIPE. The model consists of 440 pipe elements, a stinger and a vessel. The vessel RAO is similar to that of the S-lay vessel Solitare. The stinger configuration is however not a traditional configuration. The stinger for this model is mounted near the center of gravity of the vessel. This limits the pitch response of the pipeline, as the length of the arm from the center of gravity is reduced. The pipe elements and sea state parameters were changed to fit the case description for the two pipelines at Ormen Lange.

8.3.1 Critical Installation Phase

In this thesis a worst-case scenario has been considered, when the lay vessel stops for a longer period of time, and a weld is located at the position with the largest stress range (stinger tip). In this case the weld will be more susceptible to fatigue damage than the pipe itself. The recommended accumulated fatigue damage during installation should not exceed 10% of the total fatigue life (DNV, 2010).

The following presents the time-stress signal observed at the stinger tip.

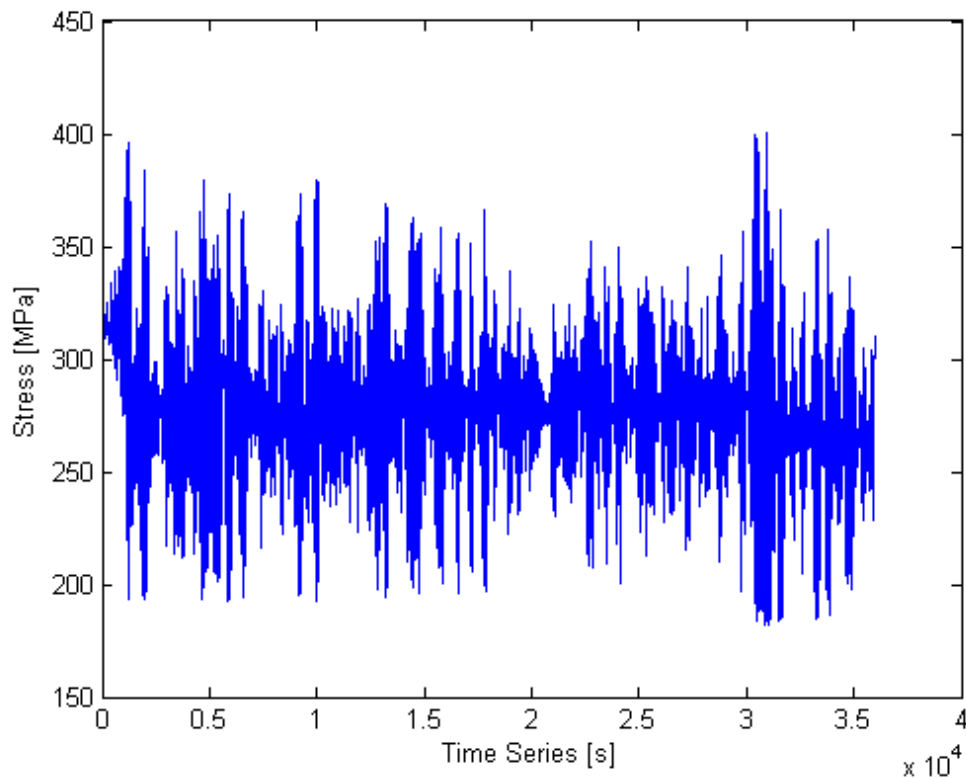


Figure 18 Stress-Time plot at the stinger tip

9 Results SIMLA

The stress-time signals from the stinger tip were run through a postprocess script written in MATLAB, where the cycles were counted using the Rainflow method. The script also calculated a bending stress for each stress range, corresponding to the weld eccentricity bending moment.

9.1 Rainflow counting and post processing

The dynamic plots from SIMLA have to be processed to extract the number of cycles and stresses needed as a input to LINKpipe. This includes a counting method for the cycles in the stress-time signal. This is done by a method referred to as Rainflow counting.

This method used four successive points along the stress signal. (S_1 , S_2 , S_3 and S_4) These points are signal turning points. The stress range between these signals is calculated, to form three stress range values (ΔS_1 , ΔS_2 and ΔS_3). If ΔS_2 is less than or equal to its two adjacent ranges (ΔS_1 and ΔS_3) the two range points (S_2 and S_3) is discarded and the cycle is represented by the range between S_1 and S_4 . If the middle range is larger than its adjacent ranges, the test moves forward to include a new point, S_5 , where it repeats itself. The ignored range, the residue, can be handled by two methods depending on the final use, decomposition into cycles for fatigue prediction and storage for sequence reconstruction. The decomposition method, which will be used in this thesis, uses two residue sequences added together. This new sequence is then run through the same rainflow procedure, to extract the remaining cycles. (Amzallag, Gerey, Robert, & Bahuaud, 1994)

The cycle count can be presented as a table listing the number of cycles and their respective stress range. Such a table may be directly imported into LINKpipe, for the fatigue analysis.

10 LINKpipe model

The input to LINKpipe from SIMLA is the cycle count, the corresponding stress ranges, and the eccentricity bending stress. In addition to the results from SIMLA, the geometry and material properties of the pipeline are included.

A finite element model of the pipe and crack is formed by specifying the mesh and crack characteristics. This implies defining a fine mesh for the area closest to the crack and a coarser mesh for the rest of the pipe section.

A cathodic protection system may be added to the fatigue analysis. The system chosen for this analysis were a -1100mV system.

10.1 ECA Parameters

A simplified ECA evaluation has been performed considering the stress ranges found by SIMLA. However, an assumption regarding the initial weld flaw has been made. The initial weld flaw is assumed to be 92 x 4 mm (Reinertsen AS, 2012). The validity of this assumption is not a part of this thesis, and is therefore a potential source of error.

10.1.1 Correction factor

The resulting crack depth from LINKpipe is given as both the realistic fatigue growth, as well as a crack depth. This crack depth is a result of a correction factor known as the Irwin correction (Berge, Fracture Design of Welded Structures, 2006). This correction takes the redistribution of the stress during crack growth, into consideration. This new distribution is dependent on the yield stress and the stress intensity factor of the material.

The results presented in Table 6 below, does not include the effect of the correction factor.

11 Results LINKpipe

The results from LINKpipe are given in the following table.

Table 6 Results LINKpipe

Analysis	H _s 1.5m					H _s 2.5m				
	T _p 5s	T _p 8s	T _p 9s	T _p 10s	T _p 13s	T _p 5s	T _p 8s	T _p 9s	T _p 10s	T _p 13s
Fatigue growth [mm]	0.00	0.00	0.00	0.01	0.02	0.00	0.00	0.02	0.05	0.10
Time to failure [h]	N/A ⁴	9369	1403	476	197	N/A ⁴	1089	261	103	48
10% of fatigue life [h]	N/A ⁴	937	140	48	20	N/A ⁴	109	26	10	5

The results presented in the table above are given as the fatigue crack growth. By stretching the stress-time signal from SIMLA, one assumes that the one hour analyzed is representative for the following hours to come. By doing this, the time to fatigue failure can be calculated to the closest hour.

It can be shown that the fatigue results follow the response curve of the vessel. As expected, the highest fatigue damage is observed in the area where the RAO showed the most response.

The 10% of fatigue life row in the table above represents the time the lay vessel can stop production without abandoning the pipeline to the seabed.

⁴ All stress range values lower than the threshold value for fatigue crack growth.

Infinite life assumed

12 Discussion, conclusion and future work

12.1 Discussion

The finite element method requires an accurate representation of the specific physical case at hand. The vessel analyzed in this thesis is a modification of an actual vessel, with a different stinger setup than usual. Here, the stinger is located off the side of the vessel. This will limit the response of the pipeline, in regards to a traditional setup with the stinger running off the aft of the vessel creating a longer arm for the response to act upon.

The extraction of cycles to failure was done by extending the stress-time signal from the one hour of analysis done. It was assumed that the one hour analysis would provide a representative distribution of stress ranges for a longer time period. The cycles extracted for the failure analysis are therefore based on the one hour used in the basic analysis. As a result of this the exact number of cycles to failure cannot be presented, and the results will be based on a hourly consideration.

No specific requirement was defined for the remaining wall thickness during fatigue crack growth. This implies that the fatigue life has a certain degree of uncertainty. However, the relationship between the analyses is still relevant, as they describe the degree of effect the different wave heights and periods have on fatigue life.

The RAO plots from the original model did not present any data for wave periods lower than 4 seconds. This was solved by extrapolating the remaining seconds and force the RAO plot to linearly approach zero. The effect of this assumption can either be conservative or non-conservative, as the realistic approach to zero is nonlinear. The degree to which this affects the response of the pipeline, is however most likely minimal as the RAO is quite small in this area.

The initial values for the crack depth, length and location, are based on experience and may not be realistic for all cases. An initial crack will give better grounds for fatigue growth as it would skip the threshold stage.

12.2 Conclusion

The conclusion drawn from the results presented are that the fatigue life consumption is closely related to the RAO of the vessel. The shortest time to failure was seen in the case of the 13 seconds period. This is consistent with the largest response observed in the RAO of the vessel. For such a sea state the pipeline has to be abandoned within 5 hours. Considering that the abandonment process also takes some time, the available waiting period could be further reduced. The probability of encountering a sea state of H_S 2.5 and T_p 13 seconds is however quite small given the JONSWAP spectrum for these parameters. The most likely period is 8 seconds. Here, it is shown that the vessel can wait for an extended period of time. This was also expected as the vessel in the model is quite large, and will not be as affected by smaller waves.

The method presented gives a good basis for the fatigue calculation of a pipeline during installation. The method will most likely be applicable to other sea states, as it is the RAO of the vessel which is the governing factor. For other sea states the JONSWAP spectrum will take on a different distribution, making a higher wave period more likely.

12.3 Future Work

Investigating several sea states may improve the understanding of fatigue effects on a pipeline during installation. Fatigue loading is usually regarded very conservative, and further investigation into the subject may help refine pipeline design and reduce cost.

An actual experiment should be performed to confirm the validity of the method. This would also define the level of accuracy which can be expected.

A fatigue calculation based on the method used in this thesis could easily be implemented in the SIMLA code. This would provide an effective indication of fatigue effects during installation.

The effect of seabed topography is also an interesting aspect which should be investigated further. An inclined seabed is likely to increase the loads imposed on the pipeline. This may cause the sagbend area to have higher cyclic stresses than the

stinger tip. Investigating this effect may provide valuable information on where a vessel can stop or not.

Investigating the effect of initial crack conditions (crack depth, length, shape and orientation) may be interesting with regards to defining welding and NDT requirements which accounts for the pipeline fatigue life.

13 Bibliography

2B1st Consulting. (2012, November 7). *2B1st Consulting*. Retrieved November 7, 2012, from <http://www.2b1stconsulting.com/pipelay-vessel/>

Amzallag, C., Gerey, J., Robert, J., & Bahuaud, J. (1994). Standardization of the Rainflow Counting method for fatigue analysis.

Askeland, D. R., & Phulé, P. P. (2006). *The Science and Engineering of Materials*.

Askeland, D., & Phulé, P. (2006). *The Science and Engineering of Materials*. (E. Veitch, Ed.) Toronto: Bill Stenquist.

B. Gross, O. L. (1965). *NASA Technical Note D-2603*. NASA.

Bai, Y., & Bai, Q. (2005). *Subsea Pipelines and Risers*. London: Elsevier.

Berge, S. (2006). *Fatigue Design of Welded Structures*. Trondheim: NTNU, Department of Marine Technology.

Berge, S. (2006). *Fracture Design of Welded Structures*. Trondheim: NTNU.

British Standards Institute. (2005). *BSI 7910:1999 - Guide to methods for assessing the acceptability of flaws in metallic structures*. BSI.

Cambridge - MIT. (2012, 11 11). *CMI MULTIDISCIPLINARY DESIGN PROJECT*.

Retrieved 11 11, 2012, from http://www-mdp.eng.cam.ac.uk/web/library/enginfo/textbooks_dvd_only/DAN/fracture/elasticPlastic/elasticPlastic.html

Department of Marine Technology. (n.d.). TMR4180 - Marine Dynamics.

DNV. (2010). *DNV-OS-F101*.

DNV. (2006). *Fracture Control for Pipeline Installation Methods Introduction Cyclic Plastic Strain - DNV-RP-F108*. DNV.

DNV. (2010). RP-C205. DNV.

DNV. (2012). *Submarine Pipeline Systems - DNV-OS-F101*. DNV.

- Faltinsen, O. (1990). *Sea Loads on Ships and Offshore Structures*. Trondheim: Cambridge.
- Giertsen, Taby, & Økland. (2010). *SIMLA Quick Start User Guide*. Trondheim: SINTEF.
- H. Tada, P. C. (1985). *The stress analysis og cracks handbook*. Saint Louis, Montana, USA: Fracture Proof Design.
- Larsen, C. M. (2009). *Marine Dynamics Compendium*. Trondheim.
- LINKftr. (2012, 06 06). *About LINKpipe*. Retrieved 01 15, 2013, from <http://www.linkftr.com/index.php/2012-05-07-11-43-00/linkpipe/about-linkpipe>
- Mathisen. (1990). *Large Displacement Analysis of Flexible and Rigid Systems Considering Displacement-Dependent Loads and Non-Linear Constraints*. Trondheim: NTNU.
- Moan, T. (2004). *Design of Offshore Structures*. Trondheim.
- Myrhaug, D. (2007). *Irregular sea*. Trondheim.
- Offshore Engineering . (2012, 11 6). *Offshore Engineering Blog*. Retrieved from <http://offshoreengineeringstudy.blogspot.no/2011/04/pipeline-installation-method.html>
- Reinertsen AS. (2012, 11 11).
- Reinertsen. (2010). *Flowline Design Approach to Obtain Reduced Intervention Costs*.
- Rice, J. R. (1972). *The Surface Crack: Physical Problems and Computational Solutions*. American Society of Mechanical Engineers.
- Schlumberger. (2012, October 26). *Schlumberger Oilfield Glossary*. Retrieved October 26, 2012, from <http://www.glossary.oilfield.slb.com/Display.cfm?Term=flowline>
- Sham, T. L. (1991). *The determination of the elastic T-stress using a higher order weight functions*. International journal of Fracture.
- Sævik, S. (2012). Trondheim: Svein Sævik.

Sævik, S., Økland, O. D., Baarholm, G. S., & Gjøsteen, J. K. (2012). *SIMLA Version 3.15.11 User Manual*. Trondheim: NTNU - Department of Marine Technology.

Y. Wang, D. M. (1992). *Evaluation of the elastic T-stress in surface cracked plates using the line-spring method*. International Journal of Fracture.

14 APPENDIX

14.1 Stress – Time plots from SIMLA

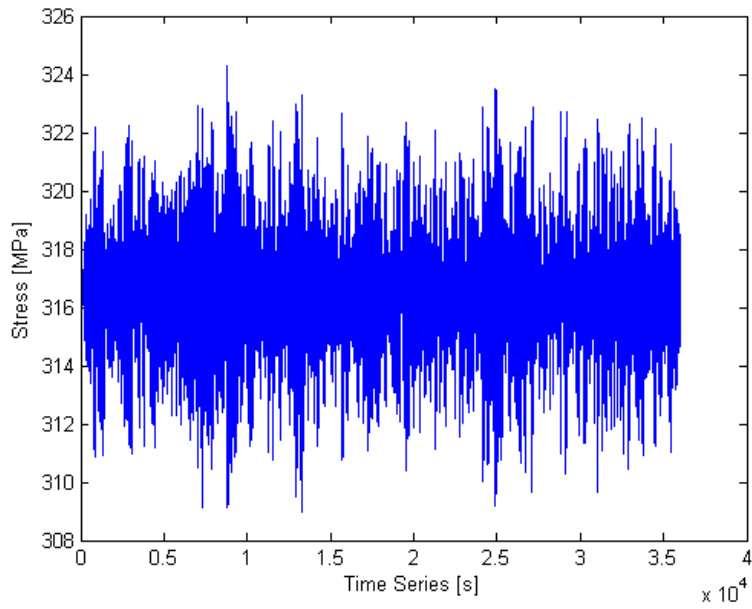


Figure 19 Hs 1.5m Tp 5s

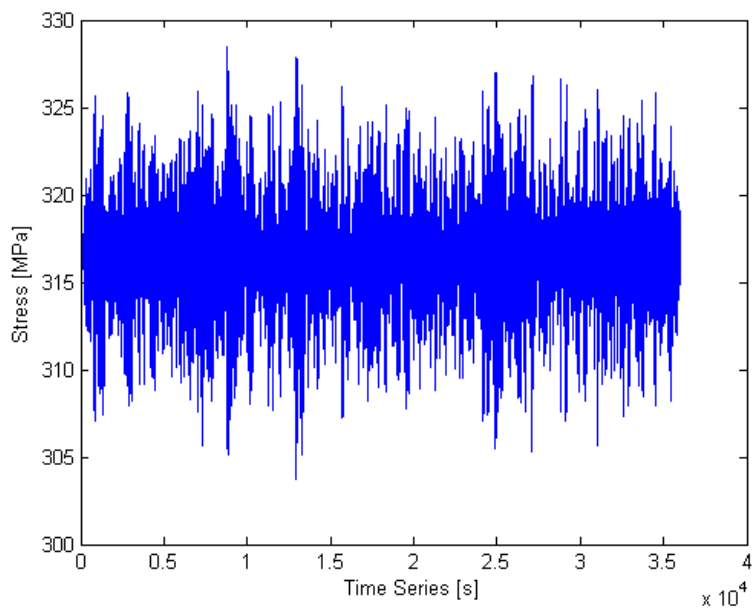


Figure 20 Hs 2.5m Tp 5s

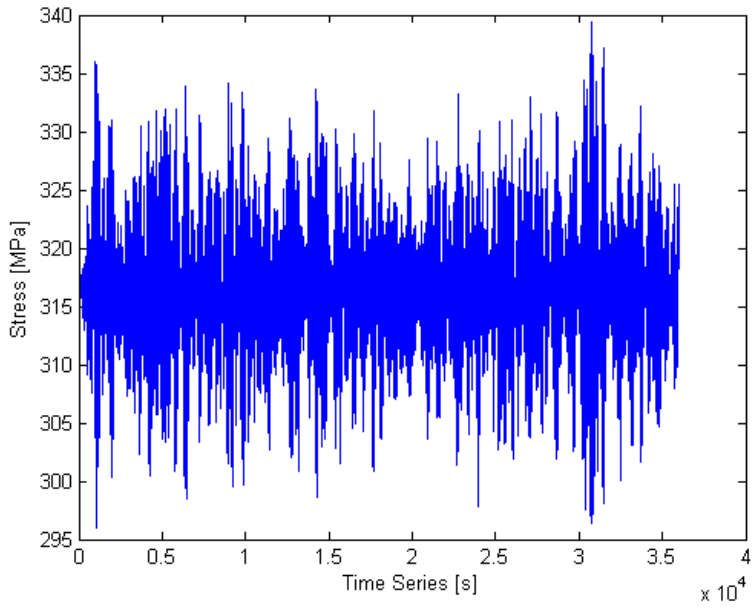


Figure 21 Hs 1.5m Tp 8s

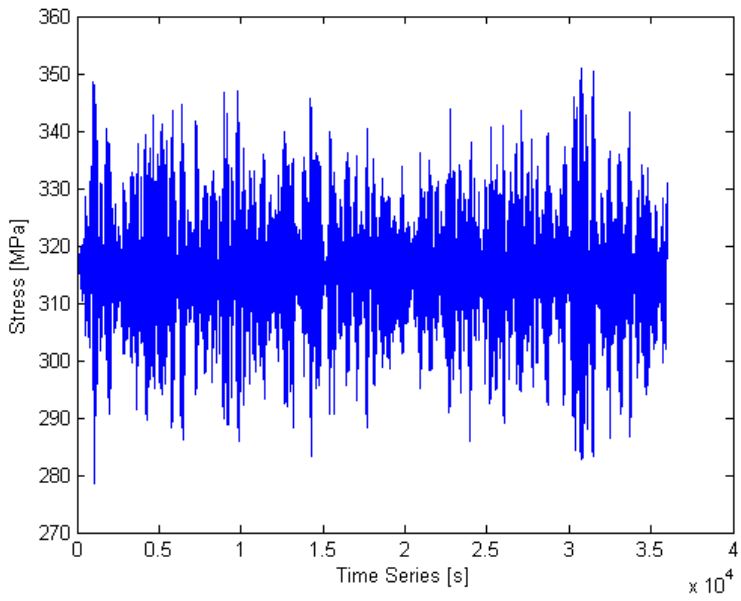


Figure 22 Hs 2.5m Tp 8s

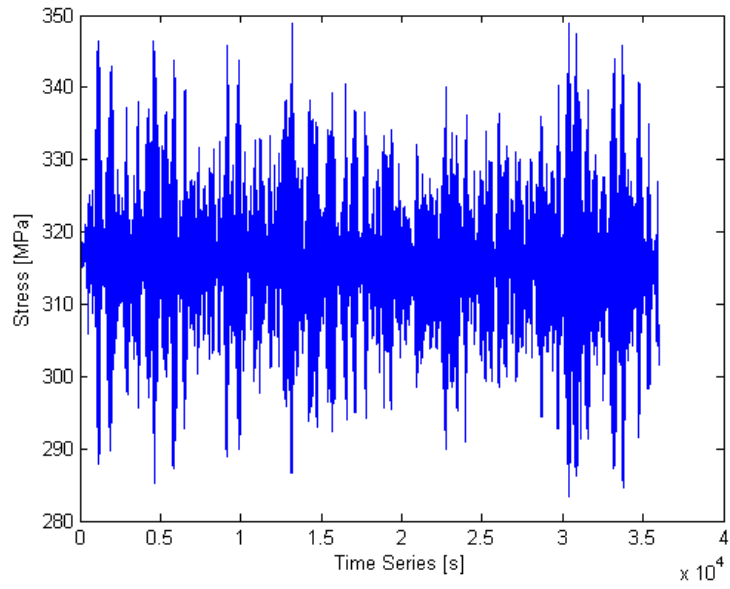


Figure 23 Hs 1.5m Tp 9s

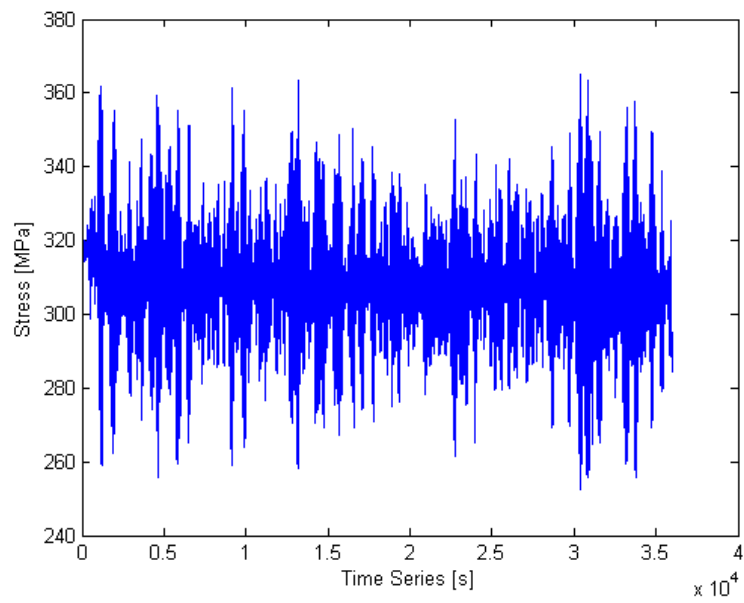


Figure 24 Hs 2.5m Tp 9s

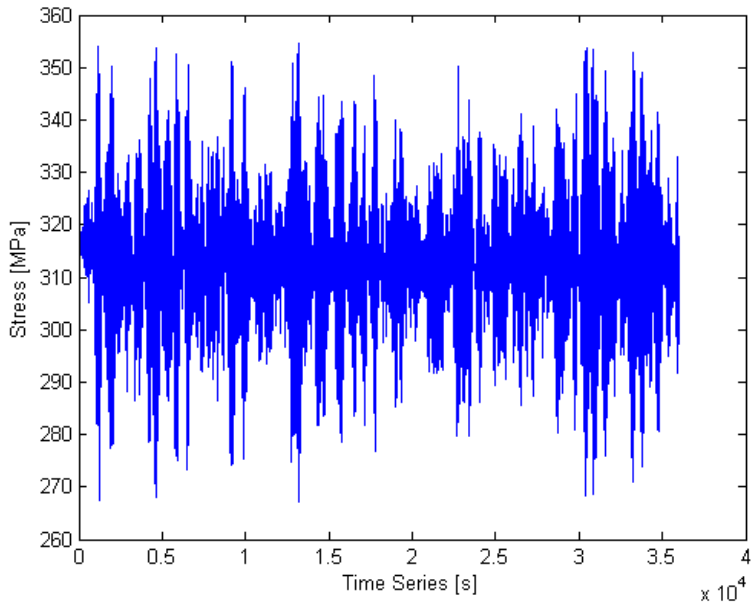


Figure 25 Hs 1.5m Tp 10s

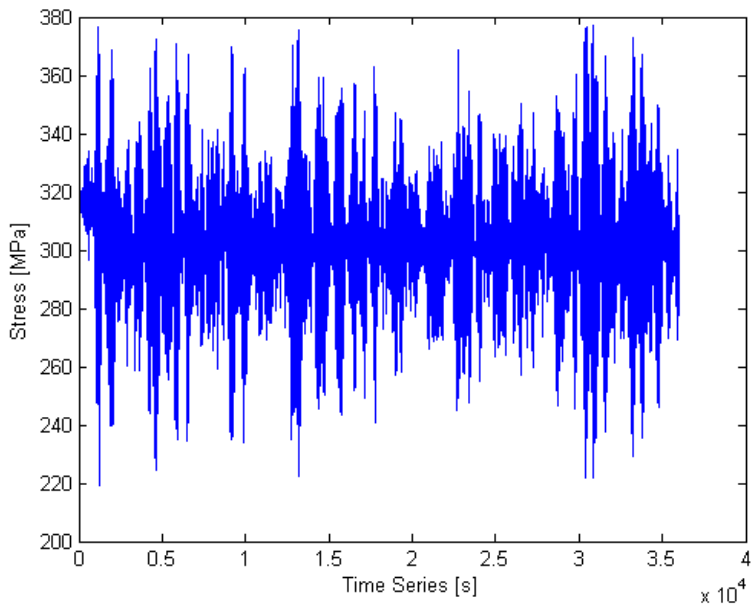


Figure 26 Hs 2.5m Tp 10s

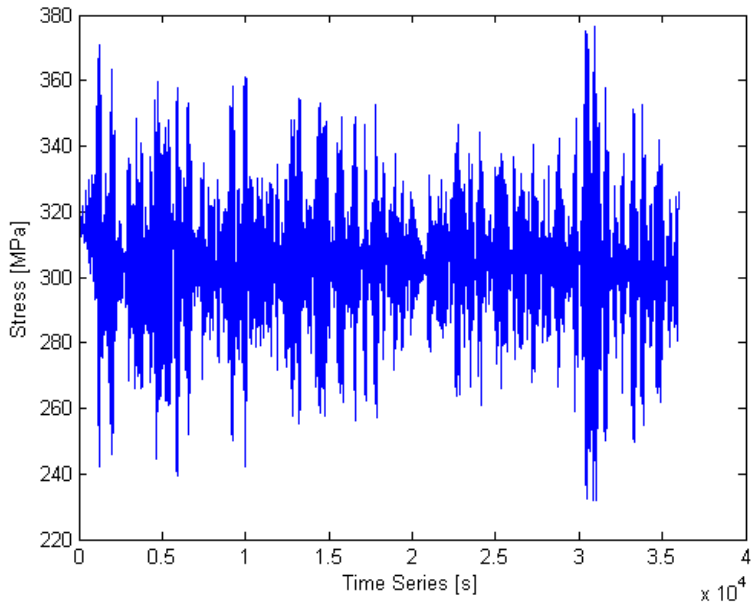


Figure 27 Hs 1.5m Tp 13s

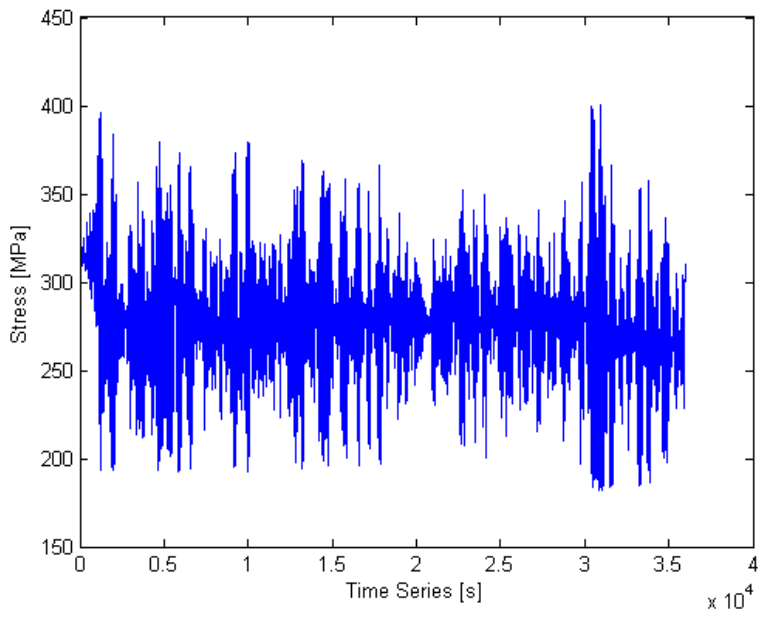


Figure 28 Hs 2.5m Tp 13s